

1 **A novel HERC4-dependent glue degrader targeting STING**

2

3 **Authors:**

4 Merve Mutlu<sup>1</sup>, Isabel Schmidt<sup>1</sup>, Andrew I. Morrison<sup>1+</sup>, Benedikt Goretzki<sup>1</sup>, Felix Freuler<sup>1</sup>, Damien Begue<sup>1</sup>, Nicolas  
5 Pythoud<sup>1</sup>, Erik Ahrne<sup>1</sup>, Sandra Kapps<sup>1</sup>, Susan Roest<sup>1</sup>, Debora Bonenfant<sup>1++</sup>, Delphine Jeanpierre<sup>1</sup>, Thi-Thanh-Thao  
6 Tran<sup>1</sup>, Rob Maher<sup>2</sup>, Shaojian An<sup>2</sup>, Amandine Rietsch<sup>1</sup>, Florian Nigsch<sup>1</sup>, Andreas Hofmann<sup>1</sup>, John Reece-Hoyes<sup>2+++</sup>,  
7 Christian N. Parker<sup>1\*</sup>, Danilo Guerini<sup>1\*</sup>

8 <sup>1</sup>Novartis Institutes for BioMedical Research, Basel, Switzerland

9 <sup>2</sup>Novartis Institutes for BioMedical Research, Cambridge, MA, USA

10 <sup>+</sup> Current position: Amsterdam UMC location Vrije Universiteit Amsterdam, Molecular Cell Biology & Immunology,  
11 Amsterdam institute for Infection and Immunity, De Boelelaan 1117, Amsterdam, The Netherlands

12 <sup>++</sup> Current position: Monte Rosa Therapeutics, Basel, Switzerland

13 <sup>+++</sup>Current position: Vector Biolog, Cambridge, MA, USA

14 <sup>\*</sup>Corresponding authors

15 **Abstract**

16 Stimulator of interferon genes (STING) is a central component of the pathway sensing the presence of cytosolic  
17 nucleic acids, having a key role in type I interferon innate immune response. Localized at the endoplasmic reticulum  
18 (ER), STING becomes activated by cGAMP, which is generated by the intracellular DNA sensor cyclic GMP-AMP  
19 synthase (cGAS). Due to its critical role in physiological function and its' involvement in a variety of diseases, STING  
20 has been a notable focus for drug discovery. Recent advances in drug discovery allow the targeting of proteins  
21 previously considered “un-druggable” by novel mechanism of actions. Molecular glue degraders are defined as the  
22 compounds leading targeted protein degradation (TPD) by creating novel ligase-substrate interactions. Here, we  
23 identified AK59 as a novel molecular glue degrader for STING. A genome-wide, CRISPR/Cas9 knockout screen  
24 showed that the compound-mediated degradation of STING by AK59 is compromised by the loss of HECT and RLD  
25 domain containing E3 ubiquitin protein ligase 4 (HERC4), ubiquitin-like modifier activating enzyme 5 (UBA5) and  
26 ubiquitin like modifier activating enzyme 6 (UBA6). While UBA5 and UBA6 could be the auxiliary factors for AK59  
27 activity, our results indicate that HERC4 is the main E3 ligase for the observed degradation mechanism. Validation  
28 by individual CRISPR knockouts, co-immunoprecipitations, as well as proximity mediated reporter assays suggested  
29 that AK59 functions as a glue degrader by forming a novel interaction between STING and HERC4. Furthermore, our  
30 data reveals that AK59 was effective on the most common pathological STING mutations that cause STING-  
31 associated vasculopathy with onset in infancy (SAVI), suggesting a potential clinical application of this mechanism.  
32 Thus, these findings not only reveal a novel mechanism for compound-induced degradation of STING but also utilize  
33 HERC4 as potential E3 ligase that for TPD, enabling novel therapeutic applications.

34 Words: 289

35 **Key words:** STING, targeted protein degradation, TPD, glue degrader, HERC4

## 36 **Introduction**

37 The cyclic GMP–AMP synthase (cGAS)–stimulator of interferon genes (STING) pathway is an important element of  
38 the innate immune system for the detection of, and the response to aberrant intracellular DNA molecules. The pathway  
39 is activated by the binding of cGAS protein to cytosolic double-stranded (DNA); this interaction initiates the  
40 production of 2'3' cyclic GMP–AMP (cGAMP) which binds to STING (previously known as TMEM173 or STING1).  
41 Located on the endoplasmic reticulum (ER) membrane in its' naive state, STING then dimerizes in the presence of  
42 cGAMP; it is translocated from the ER membrane and eventually triggers downstream interferon signaling by a  
43 cascade initiated by TANK binding kinase (TBK) phosphorylation <sup>1</sup>. The presence of double-stranded DNA in the  
44 cytoplasm is associated with viral/bacterial infection, retroviral replication and cellular stress (which could be caused  
45 by the release of mitochondrial DNA) and so the production of cGAMP, and activation of STING, acts as an innate  
46 immune response to such stimuli <sup>2</sup>.

47 Aberrant activation of cGAS/STING has been associated with numerous autoimmune diseases <sup>3</sup>. Ataxia-telangiectasia  
48 (AT), a genetic disorder linked to ATM kinase loss of function, as well as Aicardi-Goutieres syndrome (AGS), a  
49 relatively rare inflammatory disease, are among the diseases that were linked to cGAS/STING pathway activity <sup>4,5</sup>.  
50 Furthermore, individual point mutations of the STING protein are causative of STING-associated vasculopathy with  
51 onset in infancy (SAVI disease) which causes skin lesions, rashes and interstitial lung disease <sup>6</sup>. The links between  
52 the cGAS/STING pathway to multiple autoinflammatory diseases justify efforts to pharmacologically target members  
53 of this pathway <sup>3,7</sup>. As one of the main elements of this pathway, STING has been a prominent target of such efforts  
54 <sup>8,9</sup>. While a straight forward approach to STING inhibition could be targeting the cGAMP binding pocket <sup>10</sup>, which is  
55 the domain responsible for activation, there are many other mechanisms to antagonize a target protein, such as  
56 targeting post-translational modifications <sup>8</sup>.

57 Ubiquitin signaling is an important posttranslational modification (PTM) of proteins that regulates numerous signaling  
58 pathways in eukaryotic cells <sup>11</sup>. The main elements of the ubiquitin-proteasome system (UPS) consist of ubiquitin-  
59 activating enzymes (E1), ubiquitin-conjugating enzymes (E2) and ubiquitin ligases (E3). As their names suggest, the  
60 chain reaction linking ubiquitination of substrate proteins starts with ubiquitin activation via an E1 enzyme,  
61 subsequently the ubiquitin is transferred, by an E2 enzyme, from the E1 component to an E3 ligase which links  
62 ubiquitin to the target protein. The function of the E3 ligase is to create a scaffold for both the E2 and substrate for  
63 transfer of the ubiquitin to the target protein <sup>12</sup>. There are four major E3 ligase families clustered according to their  
64 functional domains and mechanism of action. A major cluster of E3 ligases, which include representatives such as  
65 APC, SCF complex or DCX complex, are members of the RING (Really Interesting New Gene)-finger containing  
66 family <sup>13,14</sup>. While RING-finger-containing E3 ligases function as scaffolds mediating close proximity between E2  
67 and the target protein, the HECT-domain-containing E3 ligases interact with ubiquitin directly, utilizing an  
68 intermediate step before ubiquitination of target protein <sup>15</sup>. HERC4 belongs to the HECT-domain containing E3 ligase  
69 family and is relatively less well characterized than the RING domain family of E3 ligases. HERC4 expression has  
70 been associated with several cancer types including breast cancer, hepatocellular carcinomas and lung tumors <sup>16–18</sup>.  
71 Additionally, only a few target substrates of HERC4 have been identified; such as Smoothed protein (SMO) <sup>19,20</sup>,

72 Salvador (SAV) protein <sup>21</sup>, c-Maf <sup>22</sup> and progesterone receptor (PGR) <sup>23</sup>. The structure and the mechanism of action  
73 of HERC4 has not yet been fully defined.

74 Interest in E3 ligases has increased tremendously over the last 20 years due the discovery of compounds that can bring  
75 about novel protein interactions with E3 ligases. Molecular glue degraders and proteolysis-targeting chimera  
76 (PROTACs) defined as compounds that mediate association of an E3 ligase to a target protein that is usually not a  
77 natural substrate of that E3 ligase. This chemically mediated protein-protein interaction (PPI) brought completely new  
78 perspective to the field of drug discovery, allowing proteins to be targeted for proteasomal degradation (TPD).

79 Our study leveraged genome-wide CRISPR/Cas9 knockout screening to enumerate the genes involved in a novel  
80 compound-directed STING degradation mechanism. This report describes the identification of the novel compound  
81 (AK59-51TB, in short AK59) that inhibits the cGAS/STING pathway via targeted proteasomal degradation of STING.  
82 A genome-wide CRISPR-Cas9 screen was conducted to identify genes inhibiting the compound-mediated STING  
83 degradation. Subsequently, the function of AK59 was shown to be dependent on HERC4, UBA5 and UBA6, each of  
84 which reduces AK59 activity when individually knocked out. Moreover, immunoprecipitation assays and a novel PPI  
85 assay revealed that the interaction between STING and HERC4 only occurs in the presence of the compound. These  
86 results identify AK59 as a glue degrader of STING and demonstrate a novel regulatory mechanism of the  
87 cGAS/STING pathway, unveiling the potential of HERC4 as an E3 ligase that has not previously been exploited for  
88 known TPD mechanisms.

## 89 **Results**

### 90 **AK59 is a selective inhibitor of STING**

91 Due to its' significance in various autoimmune diseases and cancer, the regulation of the cGAS/STING pathway is of  
92 interest to pharmaceutical companies and society<sup>3</sup>. STING is one of the main elements of this pathway and a key  
93 regulator of interferon regulatory factors (IRFs), thus regulation of STING expression may have a high potential  
94 therapeutic value in the field of immunology<sup>9</sup>. Due to this potential therapeutic application, a portion of the Novartis  
95 compound collection was screened to identify compounds that inhibit the type 1 interferon response upon expose to  
96 exogenous DNA (data not shown). THP1 human monocytic cells were chosen as a suitable cell model with detectable  
97 and relevant cGAS/STING pathway activity. Among the compounds screened, AK59 showed significant inhibitory  
98 effect on STING activity. Western blot analysis of THP1 cells showed that 16 hours of compound incubation caused  
99 a drastic decrease of STING protein levels (Figure 1A). While AK59 showed significant decrease in STING protein  
100 levels, QK50-66NB (in short QK50) treatment, a close structural analog of AK59, did not affect STING levels in  
101 treated THP1 cells (Figure 1A), highlighting the specificity of AK59. To demonstrate that STING degradation  
102 translated to downstream inhibition of the pathway, commercially available Dual-THP1-Cas9 cells (that have a Lucia  
103 luciferase reporter linked to IRF responsive promoter) were used to monitor compound effects on activation of the  
104 interferon response pathway. Upon stimulation with 30  $\mu$ M of cGAMP, Dual-THP1-Cas9 cells showed an increased  
105 luminescence signal that was significantly inhibited by treatment with 10  $\mu$ M AK59 (Figure 1B). Dual-THP1-Cas9  
106 cells in which STING had been knocked out<sup>24</sup> were used as a negative control to show the specificity of the pathway

107 activation via cGAMP stimulation. Additionally, dose response of these two related compounds showed that QK50  
108 treatment of cGAMP stimulated Dual-THP1-Cas9 cells did not show the same decrease in IRF pathway signaling  
109 (Supplementary Figure S1A). Both western blot as well as reporter assay results showed that AK59 was specifically  
110 inhibiting STING-mediated activation of the IRF pathway.

111 To further characterize the effect of AK59 on THP1 cells, an unbiased proteomics approach used. THP1 cells treated  
112 with either DMSO (vehicle), 10  $\mu$ M AK59 or 10  $\mu$ M QK50 for 16 hours and tryptic digests of total cell lysates were  
113 analyzed by LC-MS/MS (Supplementary Figure S1B). The treatment conditions were compared to the vehicle control  
114 group and fold changes were calculated accordingly. The proteomics analysis revealed significantly downregulated  
115 proteins with a  $< -1$  Log<sub>2</sub> fold decrease and a false discovery rate p-value (q value) of less than 0.01 (Figure 1C,  
116 Supplementary Table S1). Protein expression levels of STING was found to be significantly downregulated upon  
117 AK59 treatment compared to vehicle control. Furthermore, STING expression levels remained unaltered in the  
118 presence of non-functional analog of AK59, QK50 (Supplementary Figure S1C-D).

119 UPS machinery an important protein regulatory element in eukaryotic cells that plays a critical role in numerous  
120 cellular pathways<sup>25</sup>. To understand whether change of the protein levels of STING is due to proteasomal degradation,  
121 bortezomib was added prior to the compound treatment. Changes of the proteomics profile upon 50nM bortezomib  
122 addition showed that the downregulation on STING protein by AK59 were rescued (Figure 1D). To validate this  
123 finding, proteasomal degradation was inhibited using two different proteasome inhibitors (bortezomib and MG132).  
124 In addition, a neddylation inhibitor (MLN4924) was tested on AK59 treated THP1 cells (Supplementary Figure S1E).  
125 Proteasomal inhibition or neddylation inhibition was initiated 1-2 hours prior to compound treatment and maintained  
126 during the 16 hours of AK59 incubation. Interestingly, neddylation inhibition did not rescued AK59-mediated STING  
127 downregulation. While the proteasomal inhibitors were highly toxic to the cells, bortezomib showed the best rescue  
128 of the compound mediated STING degradation. Additionally, two concentrations of bortezomib treatment (25 and 50  
129 nM) were selected as having the largest effect on proteasomal inhibition without causing excessive cell death when  
130 combined with various doses of AK59. The STING protein levels in THP1 cells that measured by FACS (Figure 1E)  
131 showed that proteasomal inhibition via bortezomib rescues compound-derived STING degradation to a certain extend  
132 in a dose dependent manner. Furthermore, ubiquitination pulldown assays showed STING ubiquitination upon AK59  
133 (Figure 1F). These findings corroborated an inhibitory effect of AK59 on STING and therefore cGAS/STING  
134 signaling, via induced UPS.

### 135 **Lysine 150 of STING is essential for AK59-mediated STING degradation**

136 To dissect the functional domain(s) of STING essential for novel AK59-mediated degradation, GFP tagged STING  
137 expression vectors were constructed and expressed in HEK293T cells (which do not express endogenous STING).  
138 The expression plasmids constructed were focused on the cytosolic domain of STING to avoid the complexity the  
139 transmembrane domains might introduce in folding or localization. Several constructs that contain the cytosolic  
140 domain of STING differing on the connector helix domain were created (Supplementary Figure S2). STING  
141 degradation was tracked in live cells by following GFP fluorescence after 10  $\mu$ M AK59 treatment. STING expression  
142 on STING<sup>141-341</sup>-GFP (construct #1) expressing HEK293T cells was significantly reduced while the shorter STING<sup>155-</sup>

143 <sup>341</sup>-GFP(construct #4) expressing HEK293T cells seemed not to be influenced by compound treatment (Figure 2A).  
144 This indicated that the connector helix domain of STING protein (141-155aa) appears to be involved in the function  
145 of AK59. To understand whether this domain is important in the binding or the ubiquitination of the STING protein,  
146 lysine residues at the connector helix domain were further investigated. The K150 lysine residue, located within the  
147 connector helix domain, has been linked to PTMs such as ubiquitination of STING and its degradation <sup>26,27</sup>. In order  
148 dissect the two functions of AK59 on STING (interaction vs. ubiquitination), mutation of K150 to arginine (K150R)  
149 on non-GFP tagged STING<sup>141-341</sup> construct (STING<sup>141-341\_K150R</sup>, construct #6) was introduced. Together with non-  
150 GFP tagged STING<sup>141-341</sup>(construct #5) and STING<sup>155-341</sup>(construct #7), STING<sup>141-341\_K150R</sup> construct transiently  
151 expressed in HEK293T for side-by-side comparison. Ubiquitin pulldown followed by western blot on these cell lines  
152 showed that ubiquitination levels remained constant in either STING<sup>155-341</sup> or STING<sup>141-341\_K150R</sup> expressing  
153 HEK293T, whereas ubiquitination of STING has been increased in STING<sup>141-341</sup> expressing HEK293T cells (Figure  
154 2B). These data indicated that K150 residue of STING is essential for AK59-mediated ubiquitination and therefore  
155 degradation of the protein.

156 To investigate whether AK59 functions also on pathological STING variants, cGAS/STING pathway associated  
157 diseases searched in the literature. STING-associated vasculopathy with onset in infancy (SAVI) is rare genetic  
158 autoimmune disorder caused by single point mutations on STING protein <sup>28-31</sup>. The point mutations N154S and  
159 V155M are present in the cytosolic domain of STING and are the most commonly detected causative mutations in  
160 SAVI patients <sup>32</sup>. In order to observe the effect of AK59 on SAVI mutant STING proteins, these two mutations were  
161 introduced into the STING<sup>141-341</sup>-GFP constructs (constructs #1-4, Supplementary Figure S2). After transient  
162 transfection of the wild type and mutant STING constructs, GFP signal in live cells were tracked in vehicle treated or  
163 10  $\mu$ M AK59 treated cells. Tracking of live cells revealed that, similar to STING<sup>141-341</sup>-GFP construct, both STING  
164 variants were partially degraded in the presence of AK59 treatment (Figure 2C and Figure 2D). Our data indicate that  
165 AK59 is still functional against SAVI mutants to a certain extent, and this paves the way for future translational  
166 implications of AK59.

#### 167 **AK59 function relies on HERC4, UBA5 and UBA6**

168 While identifying the necessary domains and lysine ubiquitination's for AK59-mediated STING degradation, the  
169 mechanism of action of the compound remained unknown. To investigate the mechanism of action of AK59, a pooled,  
170 genome-wide, CRISPR-Cas9, knockout screen was conducted <sup>33</sup>. The aim was to identify genes that when knocked  
171 out, significantly abrogate the effect of AK59 in reducing the levels of STING protein in THP1-Cas9 cells.

172 A FACS-based assay to monitor the levels of STING protein was developed and used as a phenotypic readout for the  
173 CRISPR-Cas9 screen. Compound concentration and incubation time were optimized according to the median fold-  
174 difference on STING staining (Figure 3A). This identified 10  $\mu$ M AK59 and a 16-hour incubation as giving a  
175 distinctive 5-to-6-fold separation in the STING protein levels in our FACS assay. After establishing the FACS-based  
176 STING assay, the CRISPR/Cas9 genome-wide screen was conducted (Figure 3B). Screening subjected cells to either  
177 DMSO (vehicle) control or 10  $\mu$ M of AK59 for 16 hours and cells were sorted according to their STING expression.  
178 "high" and "low" STING groups were assigned as the higher and lower 25% quartile of the sorted cells. Enriched



179 and depleted sgRNAs in the comparison of high vs. low STING protein levels following treatment, as well as the  
180 control group, were presented as a plot displaying RSA p-value (significance of the hits) for guides targeting each  
181 gene as well as the magnitude of this effect compared to the other genes (Q3 values) (Figure 3C, Supplementary Figure  
182 S3A-C, Supplementary Table S2). To distinguish the genes that are significantly enriched in AK59 high vs. low  
183 STING comparison and stable in DMSO high vs. low comparison, the Euclidean distance between the two sets of (Q,  
184 RSA) coordinates was calculated (Supplementary Table S2). By ranking the distances, candidate hits that are altered  
185 only in the AK59 low vs. high comparison identified. Figure 3D represents the ranked order of the genes, where their  
186 knockout resulted in higher STING protein expression in the AK59 treatment group. Among these highly ranked  
187 genes, HERC4, UBA5 and UBA6 attracted our attention. HERC4 is a HECT domain containing E3 ligase, however  
188 few of its targets have been identified and reported in the literature<sup>19-23</sup>. UBA5 and UBA6 are ubiquitin-like modifier  
189 activating E1 proteins. Individual sgRNAs targeting these three genes show that most of them indeed enriched in the  
190 AK59 treatment group with high STING expression compared to the control group (Figure 3E). Additionally,  
191 STRING analysis (Version 11.5)<sup>34</sup> revealed that interactions between UBA5, UBA6 and HERC4 had been reported  
192 in *Homo sapiens*. Importantly, none of these candidates have not been previously linked to STING (Figure 3F). These  
193 results increased our confidence on the mechanism of AK59 on STING regulation is through UPS involving HERC4,  
194 UBA5 and UBA6 as regulatory factors.

195 To validate the CRISPR genome-wide screen results, individual knockout cell lines constructed. Two best-performing  
196 sgRNAs per candidate from the genome library selected and introduced to THP1-Cas9 cells with lentiviral particles.  
197 After the third passaging of the cells following lentiviral transduction, cells were collected to check the CRISPR  
198 editing efficiency. Modification-rate on the cut-site assessed by PCR followed by tracking of indels by decomposition  
199 (TIDE) analysis<sup>35</sup> (Figure 4A, 4D and 4G). To show that the modifications on the cut sites on each gene resulted in  
200 depletion (or decrease) in protein levels these were assessed (Figure 4B, 4E, 4H and Supplementary Figure S4).  
201 ACTIN or VINCULIN proteins were used as a loading control. After confirming the loss-of-function (LoF) of each  
202 gene, the FACS based assay monitoring STING protein levels was used to further validate our screen results. HERC4,  
203 UBA5 and UBA6 sgRNA transduced THP1-Cas9 lines showed higher levels of STING protein in the presence of 10  
204  $\mu$ M AK59 treatment compared to control (Ctrl) sgRNA transduced THP1-Cas9 cells. While AK59 treatment resulted  
205 in up to 70% decreased of STING protein in the Ctrl cell line, in the HERC4, UBA5 and UBA6 LoF lines this was  
206 decrease to 50-60% (Figure 4C, 4F, 4I and Supplementary Figure S4). Furthermore, HERC4 as the second top rated  
207 hit in the CRISPR screen showed the highest rescue phenotype of AK59 treatment regarding STING expression  
208 (Figure 4J). All these data indicated that we could replicate the results of the genome-wide screen with individual LoF  
209 lines and that HERC4, UBA5 and UBA6 loss interrupts the effect of AK59 on reduction of STING protein levels.

#### 210 **AK59 act as a glue degrader modulating novel interaction between STING and HERC4**

211 UBA5 and UBA6 are E1 enzymes suggesting that they may act as accessory elements for AK59-mediated STING  
212 degradation. HERC4 was one of the top hits from the CRISPR genome-wide screen and as an E3 ligase became  
213 prioritized as having an important role in AK59 function. Furthermore, as HERC4 is an E3 ligase this offered the  
214 hypothesis that AK59 is acting as a molecular glue degrader creating a novel interaction between HERC4 and STING,

215 allowing STING to be ubiquitinated and degraded. To test this hypothesis, we first wanted to make sure not only  
216 compound-mediated STING degradation, but also cGAS/STING pathway activity was reversed by HERC4 LoF. It  
217 was previously demonstrated that the inhibitory effect of AK59 on STING protein was translated to downstream the  
218 IRF pathway (Figure 1B). To link HERC4 to AK59 functioning as a mechanism of action, HERC4 sgRNA was  
219 introduced to the Dual-THP1-Cas9<sup>24</sup> cell line to create HERC4 LoF. Validation of LoF was shown both by TIDE  
220 analysis on the cut site as well as western blot on protein level (Supplementary Figure S5A and S5B). As expected,  
221 luminescence due to cGAMP stimulation, indicating activation of the IRF pathway, gradually decreased with  
222 increasing concentrations of AK59 in the Ctrl cell line (Supplementary Figure S5C). In contrast to the control cell  
223 line, the HERC4 knockout Dual-THP1-Cas9 cell line showed higher luciferase activity in the presence of AK59  
224 indicating that the compound's inhibitory activity on IRF pathway is compromised in the absence of HERC4. Thus,  
225 absence of HERC4 interrupted the function of AK59 on STING protein levels and downstream on activation of the  
226 IRF pathway.

227 To observe the changes in the inhibition of cytosolic STING via AK59 in the absence of HERC4, the link between  
228 HERC4 and the ubiquitination of STING through AK59 were investigated. First, HERC4 was knocked out in  
229 HEK293-JumpIN-Cas9 cell line to test the HERC4 dependent AK59 activity on various STING constructs. Knockout  
230 efficiency was shown both by TIDE analysis and western blot (Supplementary Figure S5D and S5E). Furthermore,  
231 LoF cell lines were used to transiently expressed GFP-fused cytosolic domain for STING (Supplementary Figure S2).  
232 GFP signal tracking on live HERC4 LoF cells that transfected with STING-GFP constructs showed that HERC4 LoF  
233 ablates the differences in the degradation of different STING constructs (Figure 5A). In other words, degradation of  
234 cytosolic STING via AK59 has been blocked in the absence of HERC4. These results solidified the link HERC4, an  
235 E3 ligase, to compound-mediated STING degradation suggesting that AK59 could be functioning as a glue degrader.  
236 To further support this data, protein levels known substrates of HERC4 such as SMO and PGR<sup>19,20,23</sup> were measured  
237 in the presence of AK59 (Figure 5B). Both in the wildtype THP1-Cas9 cells as well as STING KO THP1-Cas9 cells,  
238 protein levels of SMO as well as PGR remained unchanged or even stabilized upon treatment suggesting that AK59  
239 function on HERC4 is STING-specific. This data is supported by the ubiquitin pulldown in STING<sup>141-341</sup> expressing  
240 HEK293T cells. As expected transiently expressed STING construct shows increased ubiquitination levels in the  
241 presence of the AK59 while ubiquitination of SMO remained stable (Figure 5C). Additionally, HERC4, as a HECT  
242 domain containing E3 ligase shown to be also degraded in the presence of AK59 (Figure 5B and 5C) which could be  
243 due to its' self-ubiquitination during the transfer of the ubiquitin domain from E2 enzyme to substrate.

244 For AK59 to act as a glue degrader, physical interaction between E3 ligase and its' novel substrate needed to be shown.  
245 In order to demonstrate that, experiments were conducted to investigate compound-dependent PPI between HERC4  
246 and STING protein. Co-immunoprecipitation of STING followed by western blot was performed on transiently  
247 STING<sup>141-341</sup> expressing HEK293T cells. HEK293T cells were treated with DMSO or AK59, 48 hours after  
248 transfection with either empty vector or STING<sup>141-341</sup> construct. Co-immunoprecipitation followed by western blots  
249 showed that only in the presence of AK59 was STING pulled down together with HERC4 (Figure 5D, 3<sup>rd</sup> lane).  
250 Consecutively, HERC4-interacting SMO protein levels are decreased supporting that AK59 alters substrate



251 recognition of HERC4. DMSO treated STING<sup>141-341</sup> expressing HEK293T lysate (Figure 5D, 2<sup>nd</sup> lane) did not show  
252 any band on the STING blot and showed no change in SMO levels indicating that the interaction between HERC4  
253 and STING is a novel interaction and depends on the presence of the compound. Additionally, STING<sup>141-341</sup>,  
254 STING<sup>155-341</sup> and STING<sup>141-341</sup> K150R expressing HEK293T cells were used to check the interaction of STING with  
255 HERC4. Interestingly, all the STING forms were found to still be interacting shown by co-immunoprecipitation upon  
256 compound incubation, which is further validating that connector helix sequence and the K150 residue of STING is  
257 only essential for the ubiquitination of the substrate but not for the interaction of the tripartite complex formed in the  
258 presence of AK59 (Supplementary Figure S6A).

259 To support the pulldown data indicating the AK59-mediated novel interaction of HERC4 and STING, by  
260 demonstrating compound-dependent proximity, a NanoBiT<sup>®</sup> complementation assay (Promega) was developed. The  
261 Nanobit complementation assay consists of a small (SmBiT) and large (LgBiT) piece of the Nanoluciferase protein,  
262 which have low affinity for each other. Only in the presence of a direct interaction of the conjugated proteins domains,  
263 can the SmBiT and LgBiT form a functional Nanoluc and produce a luminescence signal <sup>36</sup>. Expression constructs  
264 where the STING 141-341aa cytosolic domain was C-terminally conjugated with the LgBiT domain and full length  
265 HERC4, N-terminally linked to the SmBiT were created (Supplementary Figure S6B). These constructs were then  
266 transiently transfected into HEK293T cells and expression of the constructs were validated with western blot  
267 (Supplementary Figure S6B, below). 48 hours post-transfection; cells were treated with either DMSO or AK59. Time  
268 course (Figure 5E) as well as the dose-dependent (Supplementary Figure S6D) measurements showed that LgBiT and  
269 SmBiT interaction and therefore the nano luminescence signal is detected only in the presence of AK59. QK50 a non-  
270 functional analog of AK59 (Supplementary Figure S1A), was used as a negative control. Furthermore, cGAMP  
271 supplementation did not compete with AK59 (Supplementary S6B) indicating that cGAMP is not competing with  
272 AK59 or in other words AK59 is not binding to the cGAMP binding site. Specificity of the luminescence signal, only  
273 in the presence of AK59 but not in DMSO or QK50 treated groups supports the hypothesis that AK59 induces a novel  
274 PPI between STING and HERC4, consistent with the pulldown results.

275 These results are consistent with activity of AK59 as a novel STING glue degrader. Overall, these findings shows that  
276 AK59 is a novel degrader and causes a novel interaction between STING and HERC4. AK59 interacts with HERC4,  
277 a HECT domain containing E3 ligase, causing a novel interaction with STING, which results in proteasomal  
278 degradation of STING protein. This interaction results in not only the degradation of STING but also HERC4 leading  
279 to stabilization of known substrates of HERC4 (Figure 5F). Furthermore, AK59-mediated ubiquitination of STING  
280 K150 and subsequent STING degradation results in the inhibition of IRF pathway activation. Additionally, these  
281 results showed that AK59 not only degrades wild-type STING but also SAVI mutant STING proteins, with  
282 implications for translational applications of the AK59 mechanism of action for chronic STING activation.

## 283 Discussion

284 This study identified the mechanism of action of a novel glue degrader AK59, which mediates interactions between  
285 HERC4, a HECT domain E3 ligase, and a novel substrate, STING. Molecular glue degraders and bi-functional  
286 PROTACS have attracted significant interest as a means to use small-molecule-derived changes in intracellular protein

287 interactions for application to drug discovery <sup>37</sup>. Recently, Liu et al. showed the usage of a known small molecule  
288 inhibitor against STING (C-170) combined with pomalidomide to achieve a PROTAC approach on STING  
289 degradation <sup>38</sup>. While designing PROTACs from known inhibitors seemed to be a straightforward approach, specific  
290 glue degraders have significant advantages over PROTACs due to their size and therefore the easy conformity to  
291 Lipinski's rule of five. Moreover, while CRBN-based degradation has been the focus of the field, this study is the first  
292 showing HERC4 as a potential E3 ligase for targeted protein degradation. This may be the first report of a compound  
293 directing a HECT domain containing E3 ligase to bring about targeted protein degradation.

294 Proteomics and genome-wide CRISPR/Cas9 screening techniques were then used to explore the mechanism of action  
295 of AK59 in an unbiased manner. By using a non-functional analog of AK59, QK50, both in proteomics as well as  
296 one-by-one interaction assays, it has been demonstrated that the chemical structure is unique and restrained in its  
297 ability for formation of the novel tripartite complex. While the ability of the compound to form this tripartite complex  
298 (STING, HERC4 and AK59) was validated using orthogonal assays, a number of questions remained. One of which  
299 is whether by creating a novel pocket, AK59 interacts at an interface between STING and HERC4 (so called proximal  
300 mechanism of action) or if by binding only one of the proteins, AK59 results in a conformational change which creates  
301 a novel PPI (so called distal mechanism of action) (see Figure 5F). Additionally, we managed to isolate the interaction  
302 site of STING to the cytosolic domain. In addition, it appears that AK59 was not competing with cGAMP binding but  
303 the specific degron sequence needed to be further investigated. Lastly, HERC4 binding site of AK59 still remains  
304 uncertain. To investigate these issues, compound structural-activity-relationship and protein structures needs to be  
305 further investigated with carefully selected assay readouts.

306 In dissecting AK59's function, the proteomics data showed at distinct cluster of proteins that are downregulated upon  
307 compound treatment (Supplementary Table S1). Among these proteins TMEM173 (STING) showed significant  
308 decrease in AK59 treatment sample compared to DMSO control and this significant decrease diminished in  
309 bortezomib-treated samples, indicating that the degradation of STING through AK59 is dependent on the proteasome  
310 (Supplementary Table S1). This observation was further supported by observation of K150 residue ubiquitination of  
311 STING in the presence of compound (Figure 2C). While we are mainly interested in the compound-mediated STING  
312 degradation, the proteomics data also shows a number of proteins additional to STING have been downregulated by  
313 AK59 treatment. While these proteins can be further investigated, the structure of AK59 could be optimized for  
314 specificity to STING recognition/degradation. Additionally, few proteins such as heme oxygenase 1 (HMOX1),  
315 members of heat shock protein Hsp70 family (HSPA1A, HSPA6) and members of heat shock protein Hsp40 family  
316 (DNAJA4, DNAJB4) are upregulated in the proteomics data. Elevated levels of these protein could indicate that the  
317 compound causes elevated ER stress, activation of proteolysis and protein quality control system <sup>39,40</sup>.

318 This study reports the discovery of the first molecular glue degrader targeting STING, leading to inhibition of the  
319 cGAMP-activated IRF pathway. There has been numerous attempts to inhibit cGAS/STING pathway through  
320 targeting STING either via small molecule inhibitors, cGAMP derivatives or with PROTACs <sup>3,8,41</sup>. To our knowledge,  
321 there has not previously been a report describing inhibitors, or degraders of STING, shown to be functional on SAVI  
322 mutants. While, the AK59 showed lower degradation of STING protein in the SAVI mutant lines, its novel mechanism

323 as a molecular glue degrader using HERC4 as a novel E3 ligase opens new horizons for the regulation of STING in  
324 the context of autoimmune disorders.

## 325 **Material and Methods**

### 326 **Cell culture**

327 THP1 cells were cultured using Gibco RPMI-1640-Glutamax1 25mM Hepes medium (Life Technologies)  
328 supplemented with 10% FBS (PAA Laboratories), 1mM sodium pyruvate (Life Technologies) and 50  $\mu$ M  
329 mercaptoethanol (Life Technologies). Cells were passaged every 4-5 days by dilution to 0.2-0.3 million cells/ml.

330 Dual-THP1 cells were cultured using Gibco RPMI-1640-Glutamax1 medium (Life Technologies) supplemented with  
331 10% FBS (Life Technologies), 2mM L-glutamine (Life Technologies), 10mM Hepes (Life Technologies), 1mM  
332 sodium pyruvate (Life Technologies) and 50U/ml penicillin-streptomycin (Life Technologies). Cells were passaged  
333 to 0.2-0.3 million cells/ml every 4-5 days.

334 HEK293T or HEK293-JumpIN cells were cultured with Gibco DMEM with Glutamax (Life Technologies)  
335 supplemented with 10% FBS (Life Technologies), 10mM Hepes (Life Technologies) and 50U/ml penicillin-  
336 streptomycin (Life Technologies). Cells were passaged every 3-4 days, by diluting the cells 1 to 5, after releasing the  
337 attached cells using TrypLE (Life technologies).

338 For transfection studies, TransIT-LT1 transfection reagent (Mirus) was used according to the manufacturer's protocol.  
339 For 6-well format, 1 million HEK293T cells were seeded one day before transfection. For each well, 2.5 $\mu$ g of DNA  
340 in 7.5 $\mu$ l of TransIT-LT1 transfection reagent diluted in 250 $\mu$ l optiMEM (Invitrogen). After 15 minutes of incubation  
341 of transfection reagent with DNA, mix was added dropwise on the cells. Then 48h after transfection, cells were treated  
342 with the compound of interest.

343 For lentiviral particle production,  $1 \times 10^7$  HEK293T cells were seeded on collagen coated T75 flasks (Thermo Fisher)  
344 and then 24 hours later, the cells were transfected with 1.84  $\mu$ g of DNA of interest with 2.24  $\mu$ g of ready-to-use  
345 lentiviral packaging plasmid mix (Cellecta) using Trans-IT transfection reagent (Mirus) according to the  
346 manufacturers' protocol. Subsequently, the media was changed 24 hours after transfection and lentivirus-containing  
347 supernatants collected after 72 hours. Finally, lentivirus particles were filtered using a 0.45  $\mu$ m filter (Millipore),  
348 before being concentrated 10-fold using the Lenti-X concentrator (Takara) according to the manufacturers' protocol.

### 349 **Proteomics and analysis**

350 THP1-Cas9 cells ( $2 \times 10^6$  per well in a 6-well plate) were seeded, and treated, on the same day either with 0.1% (final)  
351 DMSO, 10  $\mu$ M AK59 or 10  $\mu$ M QK50 (0.1% DMSO final) for 16 hours. Cells were collected and washed with 1x  
352 DPBS (Gibco) after compound incubation. Before proteomics analysis of the samples the conditions were checked  
353 using western blot (for more details, see western blot) to confirm targeting effects on STING.

354 TMT-labeled peptides were generated with the iST-NHS kit (PreOmics) and TMT16plex reagent (Thermo Fisher  
355 Scientific). Equal amounts of labeled peptides were pooled and separated on a high pH fractionation system with a

356 water-acetonitrile gradient containing 20 mM ammonium formate, pH 10<sup>42</sup>. Alternating rows of the resulting 72  
357 fractions were pooled into 24 samples, dried and resuspended in water containing 0.1% formic acid.

358 The LC-MS analysis was carried out on an EASY-nLC 1200 system coupled to an Orbitrap Fusion Lumos Tribrid  
359 mass spectrometer (Thermo Fisher Scientific). Peptides were separated over 180 min with a water-acetonitrile gradient  
360 containing 0.1% formic acid on a 25 cm long Aurora Series UHPLC column (Ion Opticks) with 75 µm inner diameter.  
361 MS1 spectra were acquired at 120k resolution in the Orbitrap, MS2 spectra were acquired after CID activation in the  
362 ion trap and MS3 spectra were acquired after HCD activation with a synchronous precursor selection approach<sup>43</sup>  
363 using 8 notches and 50k resolution in the Orbitrap. LC-MS raw files were analyzed with Proteome Discoverer 2.4  
364 (Thermo Fisher Scientific). Briefly, spectra were searched with Sequest HT against the *Homo sapiens* UniProt protein  
365 database and common contaminants (Sep 2019, 21494 entries). The database search criteria included: 10 ppm  
366 precursor mass tolerance, 0.6 Da fragment mass tolerance, maximum three missed cleavage sites, dynamic  
367 modification of 15.995 Da for methionines, static modifications of 113.084 Da for cysteines and 304.207 Da for  
368 peptide N-termini and lysines. The Percolator algorithm was applied to the Sequest HT results. The peptide false  
369 discovery rate was set to 1% and the protein false discovery rate was set to around 5%. TMT reporter ions of the MS3  
370 spectra were integrated with a 20 ppm tolerance and the reporter ion intensities were used for quantification. All LC-  
371 MS raw files were deposited to the ProteomeXchange Consortium<sup>44</sup> via the PRIDE partner repository with the dataset  
372 identifier PXD000000. Protein relative quantification was performed using an in-house developed R (v.3.6) script. This  
373 analysis included multiple steps; global data normalization by equalizing the total reporter ion intensities across all  
374 channels, summation of reporter ion intensities per protein and channel, calculation of protein abundance log<sub>2</sub> fold  
375 changes (L2FC) and testing for differential abundance using moderated t-statistics<sup>45</sup> where the resulting false rate  
376 discovery (FDR) p values (or q values) reflect the probability of detecting a given L2FC across sample conditions by  
377 chance alone.

### 378 **Western blotting and co-immunoprecipitation**

379 Cells were pelleted and washed with PBS (Gibco) before lysis. For western blot analysis, cell pellets were lysed with  
380 5x extraction buffer (from co-immunoprecipitation kit, Thermo), diluted to 1x with 1xPBS (Gibco) and supplemented  
381 with cOmplete protease inhibitor (Roche) for 30 minutes on ice with pulse-vortexing every five minutes. To remove  
382 cell debris, lysate was spun at 15000 g at 4°C for 15 minutes. Supernatant, containing proteins were collected in a  
383 fresh tube and protein quantification was done using Pierce BCA assay (Thermo Fisher) according to the  
384 manufacturer's protocol. Samples were prepared with NuPAGE LDS sample buffer (Invitrogen) and NuPAGE sample  
385 reducing agent (Invitrogen), boiled in 70°C for 10 minutes, loaded on pre-cast 10 well, 12 well or 15 well NuPAGE™  
386 4 to 12% Bis-Tris 1.5mm mini protein gel (Thermo Fisher) and run in 1x MES buffer (Invitrogen) for 45-50 minutes  
387 in 200V. Semi-dry transfer was done using Trans-blot turbo transfer (Biorad) with ready-made PVDF membrane-  
388 containing transfer packs according to the manufacturer's protocol. Primary antibodies used in this study were all anti-  
389 human: STING (1:1000, CST, #13647 or 1:500, Thermo Fisher, MA526030), UBIQUITIN (1:500, CST, Cat#3936),  
390 HERC4 (1:500, abcam, Cat#ab856732), UBA6 (1:1000, CST, Cat#13386), UBA5 (1:500, abcam, Cat#ab177478),  
391 SMO (1:500, abcam, Cat#ab236465) and PGR (1:250, CST, Cat#8757). As loading control ACTIN (1:500, Sigma,

392 Cat#A5441), TUBULIN (1:500, CST, Cat#2146) and VINCULIN (1:500, CST, Cat#13901) were used, as described  
393 in figure legends. HRP conjugated anti-mouse (1:2500, CST, Cat#7076) and anti-rabbit (1:2500, CST, Cat#7074)  
394 antibodies and Amersham ECL prime western blotting detection reagent (Cytiva Life Sciences) was used to detect  
395 protein levels. The ECL signal was visualized using Bio-rad ChemiDoc XRS+ and quantified using Image Lab  
396 program (Bio-rad).

397 Co-immunoprecipitation was performed using Dynabeads™ Co-Immunoprecipitation Kit (Thermo Fisher) according  
398 to the manufacturer's protocol followed by western blot, which is described above. 50ul of HERC4 antibody (abcam,  
399 Cat# ab856732) conjugated with 10mg dynabeads and for each pulldown sample 1.5mg of antibody-conjugated  
400 dynabeads were used with 50ug of protein.

401 Co-immunoprecipitation for ubiquitin pulldown was performed using Ubiquapture-Q kit (Enzo Life Sciences)  
402 according to manufacturer's protocols. To detect captured UBIQUITIN levels, instead of provided antibody from the  
403 kit, UBIQUITIN antibody from CST (mentioned above) was used.

#### 404 **IRF pathway reporter assay**

405 In order to measure IRF pathway activity, IRF-Lucia luciferase reporter system containing Dual-THP1-Cas9 cells  
406 (InvivoGen) were used. IRF pathway reporter assay was performed in clear bottom 96-well plates (TPP) where Dual-  
407 THP1-Cas9 cell line derivative cells were seeded at a cell density of 0.4 million cells/ well and stimulated with 30  $\mu$ M  
408 cGAMP immediately. After three hours stimulation, cells were treated with the indicated compounds and the luciferase  
409 measurement was performed 16-hours after compound incubation. To detect the luciferase activity, QUANTI-Luc™  
410 (Invivogen) was prepared according to the instructions on the data sheet. The reagent (50  $\mu$ l) was added to a black  
411 with clear bottom 96-well plates (Greiner, Cat#655090) where the bottom of the plate was sealed (PerkinElmer,  
412 Cat#6005199). 20  $\mu$ l of the Dual-THP1 cells from each condition pipetted on to the luminescence reagent in 96-well  
413 plate and luminescence was measured for 0.1 second with EnVision® Multimode plate reader. Fold increase in  
414 luminescence was calculated by dividing each read to its matching control group (DMSO treated) and results were  
415 plotted using Graphpad Prism 9.

#### 416 **CRISPR genome-wide screening**

417 For genome-wide CRISPR knockout screening, THP1 cells constitutively expressing Cas9 were generated by  
418 lentiviral delivery of Cas9 protein gene in pNGx-LV-c004 and selected with 5  $\mu$ g/ml blasticidin S HCl (Thermo  
419 Fisher) as previously described<sup>46</sup>. sgRNA library targeting 18,360 protein-coding genes with 5 sgRNA/gene, as  
420 previously described<sup>47</sup>. The sgRNA library was packaged into lentiviral particles using HEK293T cells as previously  
421 described<sup>47,48</sup>. Briefly,  $2.1 \times 10^7$  HEK293T cells were seeded into CellSTACK (Corning) cell culture chambers and  
422 transfected with the sgRNA library plasmid mix together with lentiviral packaging mix (Celleccta, containing psPAX2  
423 and pMD2 plasmids that encode Gag/Pol and VSV-G, respectively) using Trans-IT transfection reagent (Mirus) 24  
424 hours after seeding. Viral particles were harvested 72 hours post-transfection and quantified using LentiX qPCR kit  
425 (Clontech).



426 THP1-Cas9 cells were expanded for library transduction. On day 0, the cells were seeded and transfected to achieve a  
427 coverage of the library of at least 1000 cells/sgRNA with a multiplicity of infection (MOI) of 0.5. 5 µg/ml polybrene  
428 was used in transfection of THP1-Cas9 cells (Millipore). Transduced cells were selected with 4 µg/ml puromycin for  
429 three days and on the 4<sup>th</sup> day, cells were analyzed for RFP expression using the FACS Aria for determining  
430 transduction efficiency. After sparing the day-4 samples, the rest of the library-transduced cells were seeded for the  
431 screen with two biological replicates per condition. At day 10, cells were treated with either DMSO or 10 µM AK59  
432 and incubated for 16 hours. After compound incubation, cells were harvested, fixed, and stained for STING expression  
433 (described in detail below). Then the fraction of cells with the 25% high and 25% low level of staining for STING, in  
434 each treatment group the sorted samples were processed for genomic DNA isolation using the QIAamp DNA blood  
435 maxi kit (Qiagen) according to the manufacturer's protocol. Genomic DNA was quantified using the Quant-iT  
436 PicoGreen assay (Invitrogen) according to manufacturer's recommendations and proceeded with Illumina sequencing.

### 437 **Illumina sequencing of the library**

438 The integrated gRNA sequences were PCR amplified using primers specific to the integrated lentiviral vector sequence  
439 and sequenced using the Illumina sequencing technology. Illumina library construction was performed as previously  
440 described<sup>47</sup>. Briefly, a total of 96 µg of DNA per sample was split into 24 PCR reactions each with the volume of 100  
441 µl, containing a final concentration of 0.5 µM of each of the following primers (Integrated DNA Technologies, 5644  
442 5'-AATGATACGGCGACCACCGAGATCTACACTCGATTTCTTGGCTTTATATATCTTGTGGAAAGGA-3'  
443 and INDEX 5'-  
444 CAAGCAGAAGACGGCATAACGAGATXXXXXXXXXXGTGACTGGAGTTCAGACGTGTGCTCTTCCGATC-  
445 3', where the Xs denote a 10 base PCR-sample specific barcode used for data demultiplexing following sequencing).

446 PCR samples were purified using 1.8x SPRI AMPure XL beads (Beckman Coulter) according to manufacturer's  
447 recommended protocol and the qPCR products quantified using primers specific to the Illumina sequences using  
448 standard methods. Amplified libraries then pooled and sequenced with HiSeq 2500 instrument (Illumina) with 1x 30b  
449 reads, using a custom read 1 sequencing primer: 5645 (5'-TCGATTTCTTGGCTTTATATATCTTGTGGAAAGGAC  
450 GAAACACCG-3'), and a 1x 11b index read, using the standard Illumina indexing primer (5'-  
451 GATCGGAAGAGCACACGTCTGAACTCCAGTCAC-3'), according to the manufacturer's recommendations.

### 452 **Analysis of the CRISPR screen**

453 Sequencing analysis was performed as previously described<sup>47</sup>. In short, raw sequencing reads were converted to  
454 FASTQ format using bcl2fastq2 (version 2.17.1.14, retrieved from [http://support.illumina.com/downloads/bcl2fastq-  
455 conversion-software-v217.html](http://support.illumina.com/downloads/bcl2fastq-conversion-software-v217.html)); trimmed to the guide sequence with the fastx-toolkit (version 0.0.13, retrieved from  
456 [http://hannonlab.cshl.edu/fastx\\_toolkit/index.html](http://hannonlab.cshl.edu/fastx_toolkit/index.html)) and aligned to the sgRNA sequences in the library using bowtie<sup>49</sup>  
457 with no mismatches allowed. Differential expression of sgRNAs was calculated using DESeq2<sup>50</sup> and gene-level  
458 results were obtained using the redundant siRNA activity (RSA) algorithm<sup>51</sup>. In RSA, the rank distribution of  
459 individual sgRNAs is examined to calculate a hypergeometric enrichment score for the concerted action of each gene's



460 set of guides. This results in a gene-level p-value for significance, and we also use the lower (Q1) or upper (Q3)  
461 quartile of the guide's fold changes to represent effect size at the gene level.

462 Due to the pooled analysis approach in RSA algorithm, range of RSA and Q values in each comparison is in the similar  
463 magnitude which allow us to do further comparisons. In order to rank the hits, RSA and Q values from two different  
464 comparisons (in this case DMSO high vs. low STING and AK59 high vs. low STING) were taken as point coordinates.  
465 Between two coordinates (aka RSA and Q values of each comparison) the Euclidean distance were calculated as the  
466 magnitude of the vector and the direction of the vector was assigned by the increase/decrease of RSA and Q values  
467 between two points (Bioconductor 4.0.2). Then, hits were ranked according to the magnitude and the direction of  
468 their vector.

469 STRING analysis was performed only between 3 selected hits (HERC4, UBA5 and UBA6) and STING to represent  
470 the relation of the genes with each other (STRING version 11.5)<sup>34</sup>.

#### 471 **STING quantification by flow cytometry**

472 THP1-Cas9 cells were seeded at a density of  $1 \times 10^6$  cells/ml in 24 well plates with the media containing the indicated  
473 compound. Compound incubation time varied between 5-16 hours and bortezomib treatments were always 1 hour  
474 prior to any additional compound treatment. Cells were always seeded together with the initial treatment. After the  
475 compound incubation, cells were collected and fixed using 2.5% paraformaldehyde (stock 32%; # 15714-S; Electron  
476 Microscopy Sciences) at 37°C for 10 minutes. Cells were then washed using FACS Wash Buffer containing 1x D-  
477 PBS + 0.5% FBS + 2mM EDTA and permeabilized at room temperature for 20 minutes using 100 $\mu$ L of Perm/Wash  
478 I (BD # 557885), diluted 1:10 with 1x D-PBS. Cell washing was performed again and then samples were stained with  
479 150 $\mu$ L/sample anti STING Alexa488; 1:200 (anti TMEM173; Abcam # ab198950) diluted in Robosep Buffer, which  
480 contained PBS + 2.0% FBS + 1mM EDTA (Stemcell; # 20104) at 4°C for 1-2 hours. After antibody incubation, cells  
481 were washed with Wash Buffer three times then cell pellets were resuspended in FACS Wash Buffer and flow  
482 cytometry acquisition on Fortessa was then performed. Analysis was performed using FlowJo software (version  
483 10.6.1)

#### 484 **Individual CRISPR knockouts and TIDE analysis**

485 THP1-Cas9, Dual-THP1-Cas9<sup>24</sup> and HEK293-JumpIN-Cas9 cells were generated by lentiviral delivery of Cas9  
486 protein gene in pNGx-LV-c004<sup>46</sup> and selected with 5  $\mu$ g/ml blasticidin S HCl (Thermo Fisher). Individual knockouts  
487 were generated by lentiviral delivery of sgRNAs in the pNGx-LV-g003 backbone. SgRNA transduced cells were  
488 selected with 3.5  $\mu$ g/ml puromycin (Thermo Fisher). sgRNA sequences targeting the gene of interests are listed below.  
489 Knockout efficiency checked by both Tracking of Indels by Decomposition (TIDE) analysis<sup>35</sup> and western blot.

490 To check the rate of Indel formation at the CRISPR cut site, TIDE analysis<sup>35</sup> was used as previously described<sup>52</sup>.  
491 Briefly, genomic DNA was extracted from approximately 1 million cells per condition using DNA extraction kit  
492 (Qiagen) according to the manufacturer's recommendations. DNA concentration is measured with Nanodrop (Thermo  
493 Fisher), and PCR reaction was performed with 2x Phusion polymerase master mix (Thermo Fisher), 5% DMSO, 100ng

494 of DNA and final concentration of 1  $\mu$ M forward and reverse primer. PCR primers for each gene listed below.  
 495 Amplification run was initial denaturation in 98°C 30 seconds, 30 cycles of 98°C 5 seconds, 61°C 10 seconds, 72°C  
 496 15 second and final extension of 72°C for 2 minutes. PCR samples were cleaned up using PCR and Gel extraction kit  
 497 (Qiagen) according to the manufacturer's protocol and Sanger sequenced.

<i>Name</i>	<i>Sequence</i>
<i>Ctrl sgRNA</i>	5'-GTAGCGAACGTGTCCGGCGT-3'
<i>HERC4 sgRNA 1</i>	5'-CCAGTCATGAAATAAACCCA-3'
<i>HERC4 sgRNA 2</i>	5'-GTAGACTGCCCATTATAG-3'
<i>UBA6 sgRNA 1</i>	5'-GCTGAAATGCTGACAAGATG-3'
<i>UBA6 sgRNA 2</i>	5'-GCTGAAATGCTGACAAGATG-3'
<i>UBA5 sgRNA 1</i>	5'-GAGGCGTCCTGTTCTTCCTG-3'
<i>UBA5 sgRNA 2</i>	5'-AGACACAGCAATGCAGAAGA-3'
<i>HERC4 sgRNA 1 TIDE forward primer</i>	5'-GCCATCTGTCTGTAAATTGTGA-3'
<i>HERC4 sgRNA 1 TIDE reverse primer</i>	5'-TCTCCTGTTACTATGACTCCTCA-3'
<i>HERC4 sgRNA 2 TIDE forward primer</i>	5'-ACTCTAGGCAGCACACTTCT-3'
<i>HERC4 sgRNA 2 TIDE reverse primer</i>	5'-CCTCCCACTGGTATGTAGCC-3'
<i>UBA6 sgRNA 1 TIDE forward primer</i>	5'-GCCCCITCCTACCTTCCAG-3'
<i>UBA6 sgRNA 1 TIDE reverse primer</i>	5'-GCCAGAACTGAGAAAGCCCT-3'
<i>UBA6 sgRNA 2 TIDE forward primer</i>	5'-TTGTGGCAAATCTGGAGCAC-3'
<i>UBA6 sgRNA 2 TIDE reverse primer</i>	5'-TGCATAATCACAACACCAGAG-3'
<i>UBA5 sgRNA 1&amp;2 TIDE forward primer</i>	5'-GCATTGAAACGAATGGGAAT-3'
<i>UBA5 sgRNA 1&amp;2 TIDE reverse primer</i>	5'-TGGGTGGGGATATGTCTCA-3'

498

#### 499 **STING-GFP construct design and tracking with live cell imaging**

500 Cytosolic domains for STING (consisting of either the C-terminal 141-341aa or 155-341aa) were cloned into the  
 501 pcDNA3.1(+) (Thermo Fisher) vector backbone with a C terminal GFP tagging. HEK293T cells were seeded on 6-  
 502 well plates (TPP) with a cell density of 1 million cells/well. One day after seeding, cells were transfected with the  
 503 STING-GFP expression constructs using the Trans-IT transfection reagent (Mirus). After transfection, cells were  
 504 placed into an Incucyte® (Sartorius) live cell imager. 48-hour after transfection, cells were treated with either DMSO  
 505 or 10  $\mu$ M AK59. Cells were treated with compound for 16 hours. Live cell analysis was performed using Incucyte  
 506 software where 10x phase contrast and GFP images were taken of each well every 30-45 minutes; 16 frames were set  
 507 on each well for even quantification and data is normalized to start of the treatment. For the HERC4 knockout and  
 508 Ctrl sgRNA comparison, all the wells were treated with the AK59 and the GFP signal difference between STING<sup>155-</sup>  
 509 <sup>341</sup> and STING<sup>141-3431</sup> was measured.

#### 510 **Nanobit complementation assay**

511 Full length human HERC4 (CCDS41533) was cloned into the pFN35K SmBiT TK-neo Flexi® Vector, N-terminal  
 512 small bit (SmBiT) tagged construct (Promega), with the native HSV-TK promoter swapped out for a CMV promoter.  
 513 Cytosolic domain of human STING (141-341aa) was cloned in pFC34K LgBiT TK-neo Flexi® Vector, C-terminal  
 514 large bit (LgBiT) tagged construct (Promega) which is transcribed under control of the HSV-TK promoter.

515 Next,  $4 \times 10^4$  HEK293T cells were seeded into of 96-well plates (TPP). On the same day, cells were transiently  
516 transfected with both of the constructs using Trans-IT transfection reagent (Mirus) according to the manufacturer's  
517 recommended protocol. Then 48 hours after transfection, cells were treated indicated doses of with either DMSO,  
518 AK59 or YJX209. Luminescence activity was the measured 30 minutes, 5 hours, 8 hours and 12 hours after compound  
519 incubation. For the dose response, all samples were measured at 16-hour post compound treatment. For the cGAMP  
520 competition with AK59, cGAMP stimulation was initiated by the addition of 30  $\mu$ M of cGAMP three hours prior to  
521 the 16-hour compound treatment. To detect the luciferase activity, Nano-Glo® luciferase assay system (Promega) was  
522 used according to manufacturer's protocol and luminescence was measured for 0.1 second with EnVision® Multimode  
523 plate reader. Fold increase in luminescence was calculated by dividing each read to its matching control group (DMSO  
524 treated) and results were plotted using Graphpad Prism 9.

## 525 **Statistics**

526 Statistical analysis of the indicated data was performed using Graphpad Prism 9. Data points were represented as the  
527 mean  $\pm$  standard deviation (SD). Appropriate statistical test for each data indicated in the figure legends.

## 528 **Acknowledgments**

529 This work was supported by Discovery Postdoc Program in Novartis Institutes of BioMedical Research (NIBR)  
530 Postdoc Office.

## 531 **Author information**

### 532 **Authors and affiliations**

#### 533 **Novartis Institutes for BioMedical Research, Basel, Switzerland**

534 Merve Mutlu, Isabel Schmidt, Benedikt Goretzki, Felix Freuler, Damien Begue, Nicolas Pythoud, Erik Ahrne, Sandra  
535 Kapps, Susan Roest, Delphine Jeanpierre, Thi-Thanh-Thao Tran, Amandine Rietsch, Florian Nigsch, Andreas  
536 Hofmann, Christian N. Parker, Danilo Guerini

#### 537 **Novartis Institutes for BioMedical Research, Cambridge, MA, USA**

538 Rob Maher, Shaojian An,

#### 539 **Amsterdam UMC location Vrije Universiteit Amsterdam, Molecular Cell Biology & Immunology, Amsterdam** 540 **institute for Infection and Immunity, De Boelelaan 1117, Amsterdam, The Netherlands**

541 Andrew I. Morrison

#### 542 **Monte Rosa Therapeutics, Basel, Switzerland**

543 Debora Bonenfant

#### 544 **Current position: Vector Biolog, Cambridge, MA, USA**

545 John Reece-Hoyes

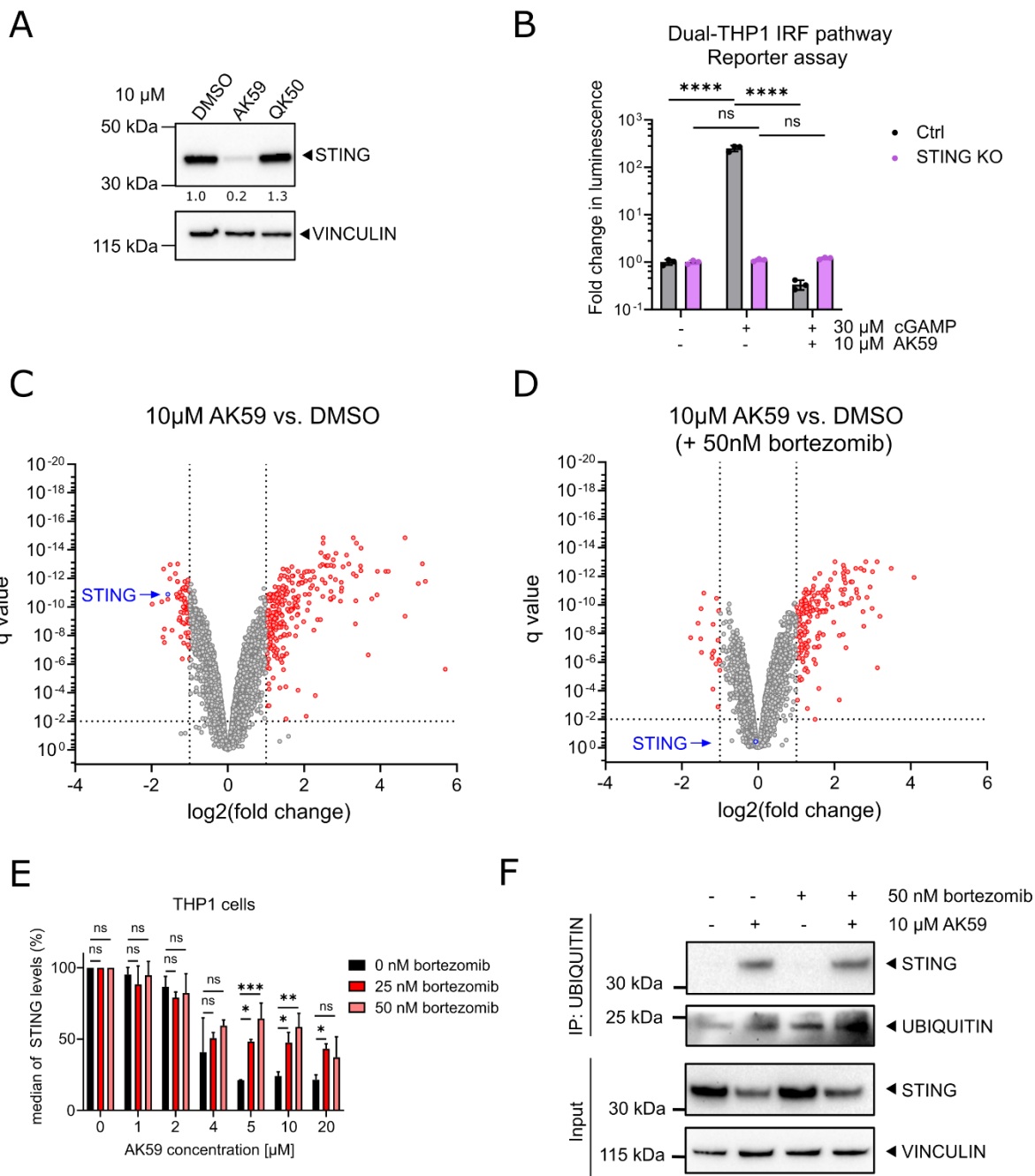
546 **Contributions**

547 M.M., I.S., A.H., C.N.P. and D.G. designed the research. M.M., I.S., A.I.M., B.G., F.F., D.B., S.K., S.R., D.B., D.J.,

548 T.T., R.M., S.A. and A.R. performed research. M.M., N.P., E.A. and A.H. analyzed data. M.M., F.N., A.H., J.R.H.,

549 C.N.P. and D.G. wrote and edited paper.

550 **Figures**

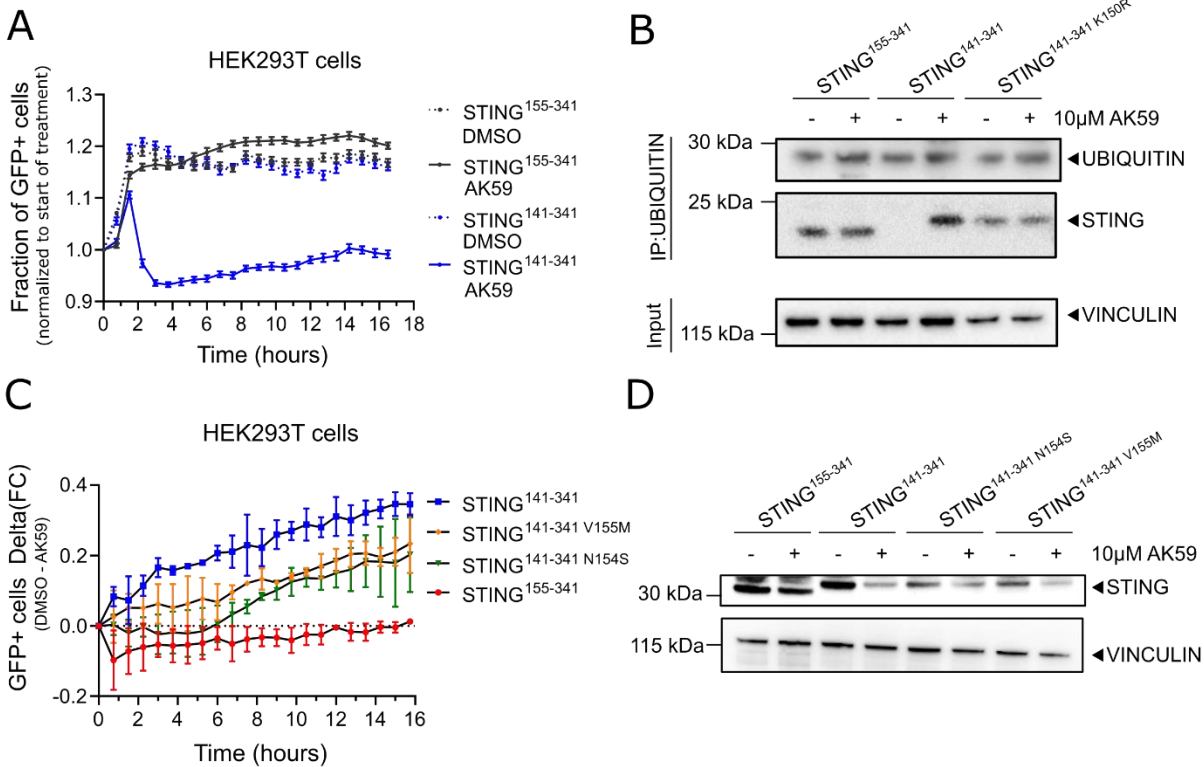


551

552 **Figure 1. AK59 decreases STING protein on THP1 cells through proteasomal degradation.** (a) Western blot  
553 showing STING protein levels in THP1 cells treated with either AK59 or QK50 for 16 hours. VINCULIN was used  
554 as a loading control. The STING expression quantified by first normalizing to its respective loading control and ratio  
555 to DMSO control. (b) IRF pathway reporter assay on wild type or STING knockout Dual-THP1-Cas9 cells. Cells  
556 were stimulated with 30  $\mu$ M cGAMP 3 hours prior to 16 hours 10  $\mu$ M AK59 incubation. Luminescence reads were  
557 normalized to the control (unstimulated) sample for each cell line. Statistical significance was calculated using two-

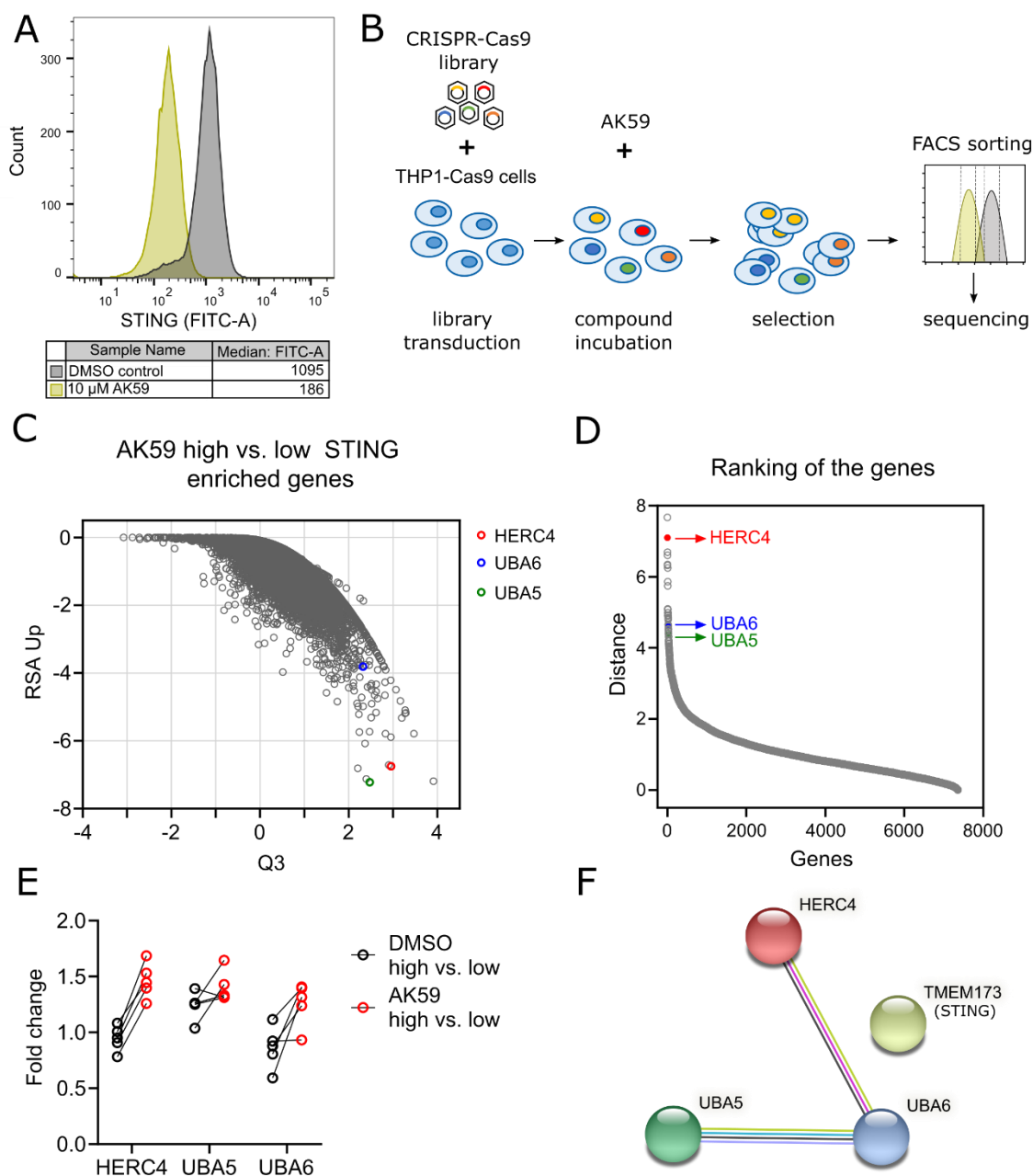
558 way ANOVA followed by Šidák's correction. Data plotted as mean  $\pm$  SD of three individual biological replicates in  
559 Graphpad Prism (Version 9). **(c-d)** Volcano plots of results from the proteomics analysis. THP1 cells were for 16  
560 hours with 10  $\mu$ M AK59 compared to control DMSO treated samples. Significantly altered protein abundances are  
561 shown with a log<sub>2</sub> fold change  $< -1$  or  $> 1$  and a q value of less than 0.01. **(e)** STING expression of THP1 cells treated  
562 with AK59 in the presence of 25nM or 50nM prior bortezomib treatment. STING expression was detected with FACS  
563 analysis on fixed cells. Bortezomib treatment was 1 hour prior to AK59 treatments. Each treatment group normalized  
564 to its individual vehicle control and represented in percentage. Three biological replicates were plotted as mean  $\pm$  SD  
565 using in Graphpad Prism (Version 9). Statistical significance was calculated using two-way ANOVA followed by  
566 Šidák's correction. **(f)** Ubiquitin pulldown followed by western blot on THP1 cells treated either 10  $\mu$ M AK59 or 50  
567 nM bortezomib or both. VINCULIN was used as a loading and pulldown control.





568

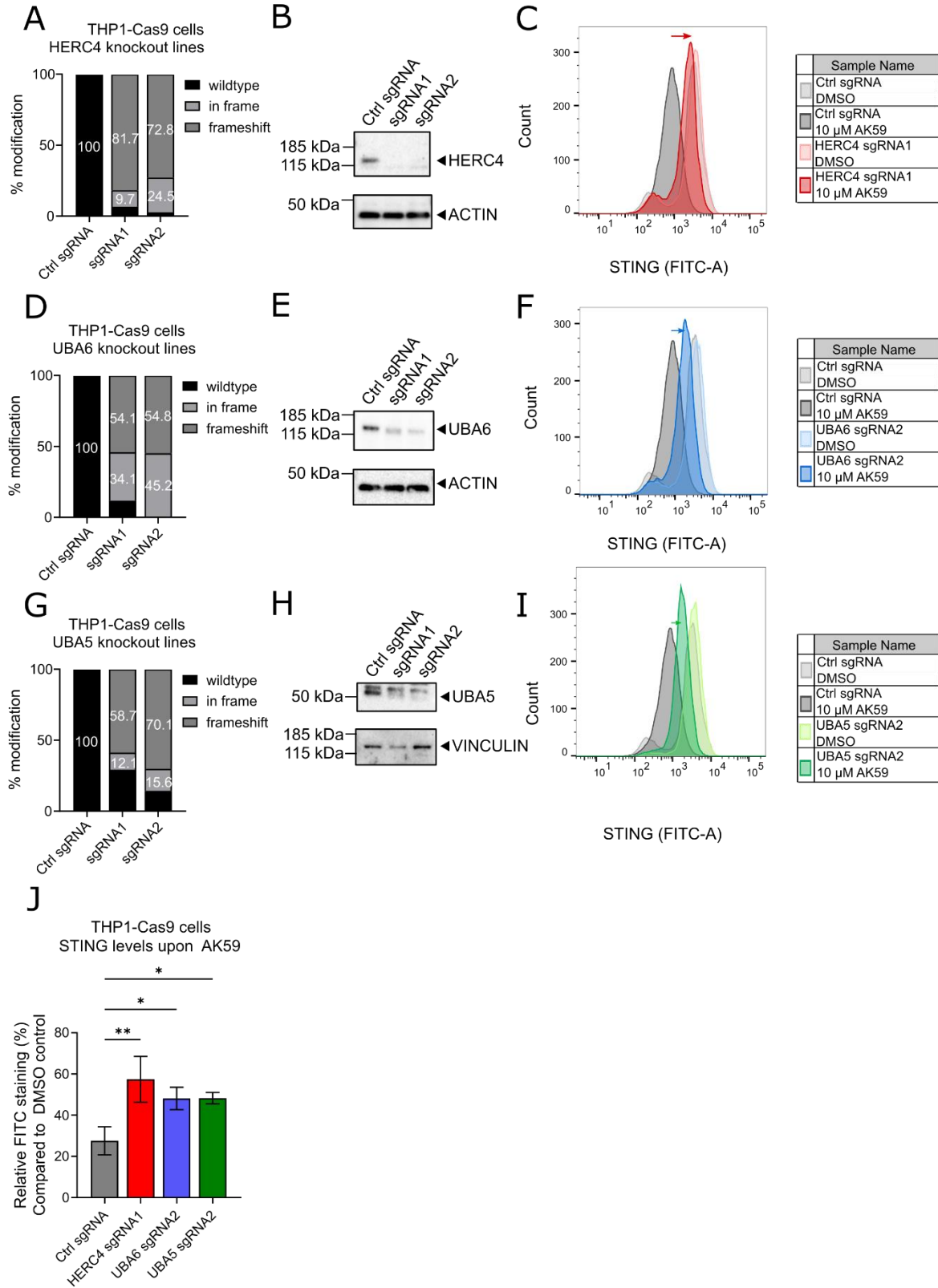
569 **Figure 2. K150 is essential for STING ubiquitination upon AK59 treatment.** (a) Live GFP positive cell tracking  
 570 of indicated STING<sup>141-341</sup>-GFP or STING<sup>155-341</sup>-GFP constructs transfected HEK293T cells upon 10 µM AK59  
 571 treatment. Data points were normalized to the start of the treatment. For each data point 16 pictures/well was taken.  
 572 Data from biological replicates were plotted as mean ± SD using in Graphpad Prism (Version 9). (b) Ubiquitin  
 573 pulldown followed by western blot on HEK293T cells transfected with the indicated STING expression constructs  
 574 and treated either 10 µM AK59 or vehicle control. VINCULIN was used as a loading and pulldown control. (c) Live  
 575 cell tracking of indicated STING-GFP constructs that harbors SAVI mutations transfected HEK293T cells after 10  
 576 µM AK59 treatment. Data points were normalized to the start of the treatment. For each data point 16 pictures/well  
 577 were taken. Data from biological replicates were plotted as mean ± SD using in Graphpad Prism (Version 9). (d)  
 578 Western blot representing the changes in STING protein levels upon AK59 treatment in SAVI mutations harboring  
 579 STING-GFP expressing HEK293T cells. Indicated constructs were transiently expressed on the cells. VINCULIN  
 580 used as a loading control.



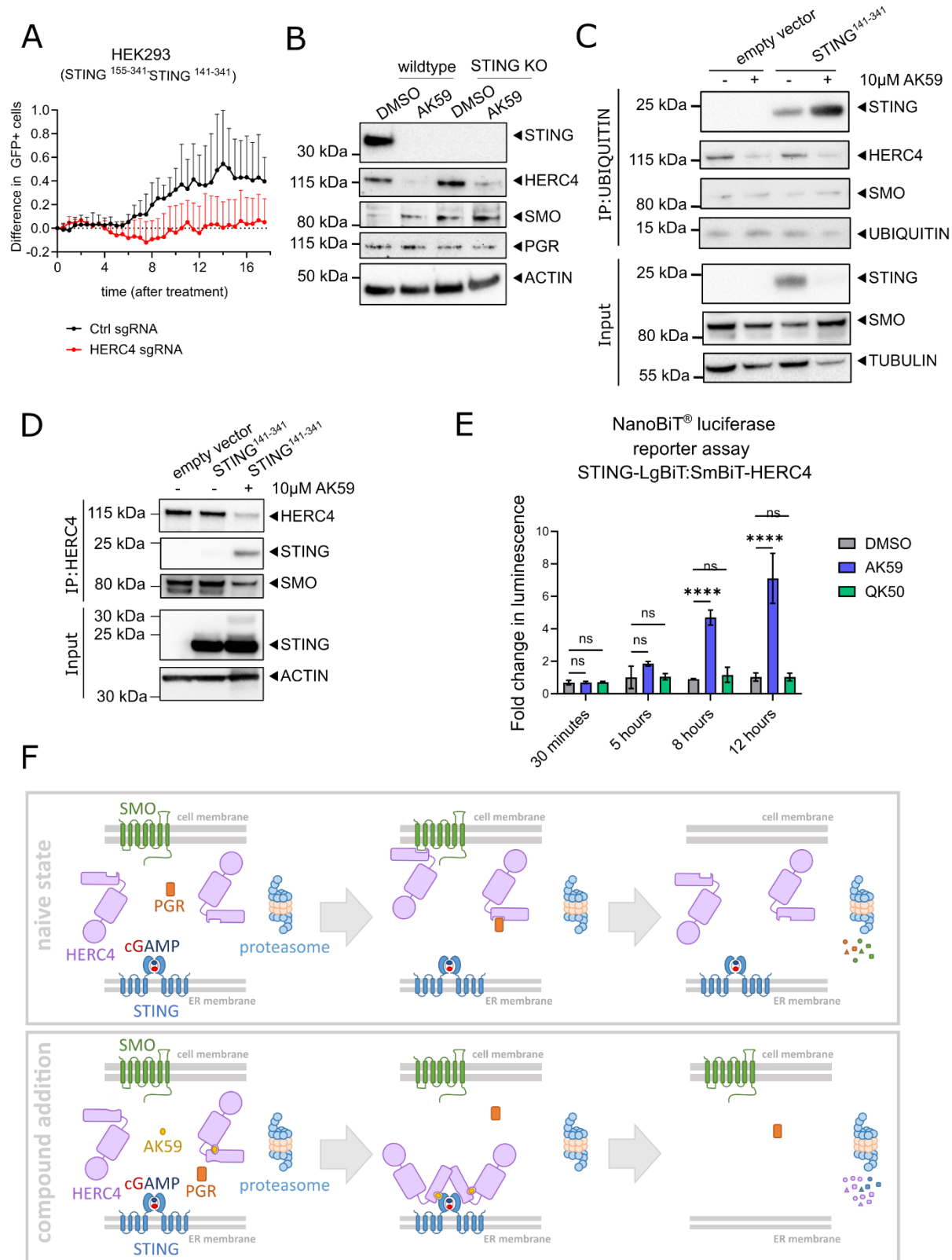
581

582 **Figure 3. CRISPR/Cas9 genome-wide screening unveiled genes responsible in AK59 activity on STING**  
583 **expression.** (a) FACS analysis of THP1-Cas9 cells that are treated either with vehicle (green) or 10  $\mu$ M AK59 (black).  
584 Experiment treated at least in three biological replicates and representative FACS reads plotted using FlowJo (Version  
585 10.6.1). (b) Schematic representation of the layout of CRISPR/Cas9 genome-wide knockout screen. (c) Comparison  
586 of RSA Up values with Q3 values from CRISPR/Cas9 screen of 10  $\mu$ M treated THP1 cells represented in a dot plot.  
587 The comparison represented in the blot is high STING expression to low STING expression in the AK59 treatment  
588 group. Each dot represents a gene from the CRISPR/Cas9 library. (d) Ranking of genes that has enriched sgRNAs in  
589 the high STING expression group compared to low. Ranking distance calculated by the change of RSA and Q values

590 between treatment groups. Each gene represented with a dot on the graph. **(e)** Individual fold changes of each sgRNA  
591 targeting HERC4, UBA5 and UBA6 in the high vs. low STING expression comparison groups in the compound  
592 treated and untreated samples. **(f)** STRING analysis representing the interaction between HERC4, UBA5, UBA6 and  
593 STING (STRING version 11.5) <sup>34</sup>.



595 **Figure 4. HERC4, UBA5 and UBA6 were validated as genes responsible for AK59 activity on STING levels. (a)**  
596 TIDE analysis of either Ctrl sgRNA, HERC4 sgRNA1 or HERC4 sgRNA2 transduced THP1-Cas9 cells. Modification  
597 rates were checked at the third passage after the initial transduction. Undefined sequencing reads were excluded. **(b)**  
598 Western blot to detect HERC4 protein levels of either Ctrl sgRNA, HERC4 sgRNA1 or HERC4 sgRNA2 transduced  
599 THP1 cells. Proteins from each cell line collected at the third passage after the initial transduction. **(c)** FACS analysis  
600 of STING expression on Ctrl sgRNA or HERC4 sgRNA1 transduces THP1-Cas9 cells that were treated either with  
601 vehicle (gray and pink) or 10  $\mu$ M AK59 (black and red). The effect of the knockout indicated with a red arrow.  
602 Experiment repeated at least in three biological replicates and representative FACS reads plotted using FlowJo  
603 (Version 10.6.1). **(d)** TIDE analysis from either Ctrl sgRNA, UBA6 sgRNA1 or UBA6 sgRNA2 transduced THP1-  
604 Cas9 cells. Modification rates were check at the third passage after the initial transduction. Undefined sequencing  
605 reads were excluded. **(e)** Western blot to detect UBA6 protein levels on either Ctrl sgRNA, UBA6 sgRNA1 or UBA6  
606 sgRNA2 transduced THP1-Cas9 cells. Proteins from each cell line collected at the third passage after the initial  
607 transduction. **(f)** FACS analysis of STING expression on Ctrl sgRNA or UBA6 sgRNA2 transduces THP1 cells that  
608 are treated either with vehicle (gray and light blue) or 10  $\mu$ M AK59 (black and dark blue). The effect of the knockout  
609 indicated with a blue arrow. Experiment repeated at least in three biological replicates and representative FACS reads  
610 plotted using FlowJo (Version 10.6.1). **(g)** TIDE analysis from either Ctrl sgRNA, UBA5 sgRNA1 or UBA5 sgRNA2  
611 transduced THP1-Cas9 cells. Modification rates were check at the third passage after the initial transduction.  
612 Undefined sequencing reads were excluded. **(h)** Western blot to detect UBA5 protein levels on either Ctrl sgRNA,  
613 UBA5 sgRNA1 or UBA5 sgRNA2 transduced THP1-Cas9 cells. Proteins from each cell line collected at the third  
614 passage after the initial transduction. **(i)** FACS analysis of STING expression on Ctrl sgRNA or UBA5 sgRNA2  
615 transduces THP1-Cas9 cells that were treated either with vehicle (gray and light green) or 10  $\mu$ M AK59 (black and  
616 dark green). The effect of the knockout indicated with a green arrow. Experiment repeated at least in three biological  
617 replicates and representative FACS reads plotted using FlowJo (Version 10.6.1). **(j)** Relative STING expressions in  
618 indicated THP1-Cas9 cell lines. Data is normalized vehicle treated group and three biological replicates were plotted  
619 as mean  $\pm$  SD using in Graphpad Prism (Version 9). Statistical significance was calculated using one-way ANOVA  
620 followed by Dunnett's multiple comparison test.



621



622 **Figure 5. AK59 acts as a glue degrader targeting STING.** (a) Live cell tracking of wildtype or HERC4 knockout  
623 HEK293-JumpIN-Cas9 cells after 10  $\mu$ M AK59 treatment. Data points were normalized to the moment of AK59  
624 treatment and to their corresponding vehicle control group. For each data point 16 pictures/well were taken. Data from  
625 biological replicates were plotted as mean  $\pm$  SD using in Graphpad Prism (Version 9). (b) Western blot showing  
626 STING, HERC4, SMO and PGR protein levels in THP1 cells treated with either AK59 or vehicle control for 16 hours.  
627 ACTIN was used as a loading control. (c) Ubiquitin pulldown followed by western blot on HEK293T cells transfected  
628 with the indicated STING expression constructs and treated either 10  $\mu$ M AK59 or vehicle control. TUBULIN was  
629 used as a loading and pulldown control. (d) Co-immunoprecipitation followed by western blot on HEK293T cells  
630 transiently expressing indicated STING expression constructs and treated either with 10  $\mu$ M AK59 or vehicle control.  
631 ACTIN was used as a loading and pulldown control. (e) Nanobit complementation assay on STING-LgBiT and  
632 SmBiT-HERC4 expressing HEK293T cells treated with either 10  $\mu$ M AK59, 10  $\mu$ M QK50 or vehicle control.  
633 Luminescence detected at the indicated time points after the start of the compound treatment. Luminescence reads  
634 were normalized to corresponding DMSO control. Three biological replicates were plotted as mean  $\pm$  SD using in  
635 Graphpad Prism (Version 9). Statistical significance was calculated using two-way ANOVA followed by Šidák's  
636 correction. (f) Graphical representation of naive and compound added state of the cells and the suggested new protein-  
637 protein interactions in the presence of AK59.

638       **References**

- 639    1.     Kato, Y., Kumanogoh, A., Takamatsu, H. & Park, J. 25 Stimulator of interferon genes (sting) plays a crucial  
640        role in type-i ifn production induced by the sera from sle patients. in (2017). doi:10.1136/lupus-2017-  
641        000215.25.
- 642    2.     Wan, D., Jiang, W. & Hao, J. Research Advances in How the cGAS-STING Pathway Controls the Cellular  
643        Inflammatory Response. *Frontiers in Immunology* (2020) doi:10.3389/fimmu.2020.00615.
- 644    3.     Decout, A., Katz, J. D., Venkatraman, S. & Ablasser, A. The cGAS–STING pathway as a therapeutic target  
645        in inflammatory diseases. *Nature Reviews Immunology* (2021) doi:10.1038/s41577-021-00524-z.
- 646    4.     Yan, N. Immune diseases associated with TREX1 and STING dysfunction. *J. Interf. Cytokine Res.* (2017)  
647        doi:10.1089/jir.2016.0086.
- 648    5.     Aguado, J. *et al.* Inhibition of the cGAS-STING pathway ameliorates the premature senescence hallmarks of  
649        Ataxia-Telangiectasia brain organoids. *Aging Cell* (2021) doi:10.1111/acel.13468.
- 650    6.     Wang, Y., Wang, F. & Zhang, X. STING-associated vasculopathy with onset in infancy: a familial case  
651        series report and literature review. *Ann. Transl. Med.* (2021) doi:10.21037/atm-20-6198.
- 652    7.     Motwani, M., Pesiridis, S. & Fitzgerald, K. A. DNA sensing by the cGAS–STING pathway in health and  
653        disease. *Nature Reviews Genetics* (2019) doi:10.1038/s41576-019-0151-1.
- 654    8.     Haag, S. M. *et al.* Targeting STING with covalent small-molecule inhibitors. *Nature* **559**, 269–273 (2018).
- 655    9.     Sheridan, C. Drug developers switch gears to inhibit STING. *Nature biotechnology* (2019)  
656        doi:10.1038/s41587-019-0060-z.
- 657    10.    Hong, Z. *et al.* STING inhibitors target the cyclic dinucleotide binding pocket. *Proc. Natl. Acad. Sci. U. S.*  
658        A. (2021) doi:10.1073/pnas.2105465118.
- 659    11.    Komander, D. & Rape, M. The ubiquitin code. *Annu. Rev. Biochem.* (2012) doi:10.1146/annurev-biochem-  
660        060310-170328.
- 661    12.    Maupin-Furlow, J. Proteasomes and protein conjugation across domains of life. *Nature Reviews*  
662        *Microbiology* (2012) doi:10.1038/nrmicro2696.
- 663    13.    Nakayama, K. I. & Nakayama, K. Ubiquitin ligases: Cell-cycle control and cancer. *Nature Reviews Cancer*  
664        (2006) doi:10.1038/nrc1881.
- 665    14.    Deshaies, R. J. & Joazeiro, C. A. P. RING domain E3 ubiquitin ligases. *Annual Review of Biochemistry*  
666        (2009) doi:10.1146/annurev.biochem.78.101807.093809.
- 667    15.    Lorenz, S. Structural mechanisms of HECT-type ubiquitin ligases. *Biological Chemistry* (2018)

- 668 doi:10.1515/hsz-2017-0184.
- 669 16. Zheng, Y. *et al.* HERC4 Is Overexpressed in Hepatocellular Carcinoma and Contributes to the Proliferation  
670 and Migration of Hepatocellular Carcinoma Cells. *DNA Cell Biol.* (2017) doi:10.1089/dna.2016.3626.
- 671 17. Zeng, W. L. *et al.* Expression of HERC4 in lung cancer and its correlation with clinicopathological  
672 parameters. *Asian Pacific J. Cancer Prev.* (2015) doi:10.7314/APJCP.2015.16.2.513.
- 673 18. Zhou, H. *et al.* The expression and clinical significance of HERC4 in breast cancer. *Cancer Cell Int.* (2013)  
674 doi:10.1186/1475-2867-13-113.
- 675 19. Jiang, W. *et al.* E3 ligase Herc4 regulates Hedgehog signalling through promoting Smoothed degradation.  
676 *J. Mol. Cell Biol.* (2019) doi:10.1093/jmcb/mjz024.
- 677 20. Sun, X., Sun, B., Cui, M. & Zhou, Z. HERC4 exerts an anti-tumor role through destabilizing the oncoprotein  
678 Smo. *Biochem. Biophys. Res. Commun.* (2019) doi:10.1016/j.bbrc.2019.04.113.
- 679 21. Aerne, B. L., Gailite, I., Sims, D. & Tapon, N. Hippo stabilises its adaptor Salvador by antagonising the  
680 HECT ubiquitin ligase Herc4. *PLoS One* (2015) doi:10.1371/journal.pone.0131113.
- 681 22. Zhang, Z. *et al.* The ubiquitin ligase HERC4 mediates c-Maf ubiquitination and delays the growth of  
682 multiple myeloma xenografts in nude mice. *Blood* (2016) doi:10.1182/blood-2015-07-658203.
- 683 23. Huang, P. *et al.* SOX4 facilitates PGR protein stability and FOXO1 expression conducive for human  
684 endometrial decidualization. *Elife* (2022) doi:10.7554/eLife.72073.
- 685 24. Willemsen, J. *et al.* TNF leads to mtDNA release and cGAS/STING-dependent interferon responses that  
686 support inflammatory arthritis. *Cell Rep.* (2021) doi:10.1016/j.celrep.2021.109977.
- 687 25. Eldridge, A. G. & O'Brien, T. Therapeutic strategies within the ubiquitin proteasome system. *Cell Death  
688 and Differentiation* (2010) doi:10.1038/cdd.2009.82.
- 689 26. Zhong, B. *et al.* The Ubiquitin Ligase RNF5 Regulates Antiviral Responses by Mediating Degradation of  
690 the Adaptor Protein MITA. *Immunity* (2009) doi:10.1016/j.immuni.2009.01.008.
- 691 27. Tsuchida, T. *et al.* The ubiquitin ligase TRIM56 regulates innate immune responses to intracellular double-  
692 stranded DNA. *Immunity* (2010) doi:10.1016/j.immuni.2010.10.013.
- 693 28. Dai, Y. F., Liu, X. Y., Zhao, Z. P., He, J. X. & Yin, Q. Q. Stimulator of Interferon Genes-Associated  
694 Vasculopathy With Onset in Infancy: A Systematic Review of Case Reports. *Frontiers in Pediatrics* (2020)  
695 doi:10.3389/fped.2020.577918.
- 696 29. Liu, Y. *et al.* Activated STING in a Vascular and Pulmonary Syndrome. *N. Engl. J. Med.* (2014)  
697 doi:10.1056/nejmoa1312625.

- 698 30. Motwani, M. *et al.* Hierarchy of clinical manifestations in SAVI N153S and V154M mouse models. *Proc.*  
699 *Natl. Acad. Sci. U. S. A.* (2019) doi:10.1073/pnas.1818281116.
- 700 31. Martin, G. R. *et al.* Expression of a constitutively active human STING mutant in hematopoietic cells  
701 produces an Ifnar1-dependent vasculopathy in mice. *Life Sci. Alliance* (2019) doi:10.26508/lsa.201800215.
- 702 32. Frémond, M. L. *et al.* Overview of STING-Associated Vasculopathy with Onset in Infancy (SAVI) Among  
703 21 Patients. *J. Allergy Clin. Immunol. Pract.* (2021) doi:10.1016/j.jaip.2020.11.007.
- 704 33. Luo, J. CRISPR/Cas9: From Genome Engineering to Cancer Drug Discovery. *Trends in Cancer* (2016)  
705 doi:10.1016/j.trecan.2016.05.001.
- 706 34. Szklarczyk, D. *et al.* The STRING database in 2021: Customizable protein-protein networks, and functional  
707 characterization of user-uploaded gene/measurement sets. *Nucleic Acids Res.* (2021)  
708 doi:10.1093/nar/gkaa1074.
- 709 35. Brinkman, E. K., Chen, T., Amendola, M. & Van Steensel, B. Easy quantitative assessment of genome  
710 editing by sequence trace decomposition. *Nucleic Acids Res.* (2014) doi:10.1093/nar/gku936.
- 711 36. Cooley, R. *et al.* Development of a cell-free split-luciferase biochemical assay as a tool for screening for  
712 inhibitors of challenging protein-protein interaction targets. *Wellcome Open Res.* (2020)  
713 doi:10.12688/wellcomeopenres.15675.1.
- 714 37. Kozicka, Z. & Thomä, N. H. Haven't got a glue: Protein surface variation for the design of molecular glue  
715 degraders. *Cell Chemical Biology* (2021) doi:10.1016/j.chembiol.2021.04.009.
- 716 38. Liu, J. *et al.* Novel CRBN-Recruiting Proteolysis-Targeting Chimeras as Degradors of Stimulator of  
717 Interferon Genes with In Vivo Anti-Inflammatory Efficacy. *J. Med. Chem.* **65**, 6593–6611 (2022).
- 718 39. Liu, X. M. *et al.* Endoplasmic reticulum stress stimulates heme oxygenase-1 gene expression in vascular  
719 smooth muscle: Role in cell survival. *J. Biol. Chem.* (2005) doi:10.1074/jbc.M410413200.
- 720 40. Ran, R., Lu, A., Xu, H., Tang, Y. & Sharp, F. R. Heat-shock protein regulation of protein folding, protein  
721 degradation, protein function, and apoptosis. in *Handbook of Neurochemistry and Molecular Neurobiology:*  
722 *Acute Ischemic Injury and Repair in the Nervous System* (2007). doi:10.1007/978-0-387-30383-3\_6.
- 723 41. Liu, J. *et al.* Novel CRBN-Recruiting Proteolysis-Targeting Chimeras as Degradors of Stimulator of  
724 Interferon Genes with in Vivo Anti-Inflammatory Efficacy. *J. Med. Chem.* **65**, 6593–6611 (2022).
- 725 42. Wang, Y. *et al.* Reversed-phase chromatography with multiple fraction concatenation strategy for proteome  
726 profiling of human MCF10A cells. *Proteomics* (2011) doi:10.1002/pmic.201000722.
- 727 43. McAlister, G. C. *et al.* MultiNotch MS3 enables accurate, sensitive, and multiplexed detection of differential  
728 expression across cancer cell line proteomes. *Anal. Chem.* (2014) doi:10.1021/ac502040v.

- 729 44. Vizcaíno, J. A. *et al.* ProteomeXchange provides globally coordinated proteomics data submission and  
730 dissemination. *Nature Biotechnology* (2014) doi:10.1038/nbt.2839.
- 731 45. Ritchie, M. E. *et al.* Limma powers differential expression analyses for RNA-sequencing and microarray  
732 studies. *Nucleic Acids Res.* (2015) doi:10.1093/nar/gkv007.
- 733 46. Dejesus, R. *et al.* Functional CRISPR screening identifies the ufmylation pathway as a regulator of  
734 SQSTM1/p62. *Elife* (2016) doi:10.7554/eLife.17290.
- 735 47. Estoppey, D. *et al.* Genome-wide CRISPR-Cas9 screens identify mechanisms of BET bromodomain  
736 inhibitor sensitivity. *iScience* (2021) doi:10.1016/j.isci.2021.103323.
- 737 48. Hoffman, G. R. *et al.* Functional epigenetics approach identifies BRM/SMARCA2 as a critical synthetic  
738 lethal target in BRG1-deficient cancers. *Proc. Natl. Acad. Sci. U. S. A.* (2014)  
739 doi:10.1073/pnas.1316793111.
- 740 49. Langmead, B., Trapnell, C., Pop, M. & Salzberg, S. L. Ultrafast and memory-efficient alignment of short  
741 DNA sequences to the human genome. *Genome Biol.* (2009) doi:10.1186/gb-2009-10-3-r25.
- 742 50. Love, M. I., Huber, W. & Anders, S. Moderated estimation of fold change and dispersion for RNA-seq data  
743 with DESeq2. *Genome Biol.* (2014) doi:10.1186/s13059-014-0550-8.
- 744 51. König, R. *et al.* A probability-based approach for the analysis of large-scale RNAi screens. *Nat. Methods* **4**,  
745 847–849 (2007).
- 746 52. Francica, P. *et al.* Functional Radiogenetic Profiling Implicates ERCC6L2 in Non-homologous End Joining.  
747 *Cell Rep.* (2020) doi:10.1016/j.celrep.2020.108068.
- 748

749 **Supplementary Materials**

750 Supplementary Figure 1. Compound characterization of AK59 and QK50.

751 Supplementary Figure 2. STING constructs.

752 Supplementary Figure 3. CRISRP/Cas9 genome-wide screening results.

753 Supplementary Figure 4. HERC4, UBA5 and UBA6 are validated as genes responsible in AK59 activity on STING  
754 expression.

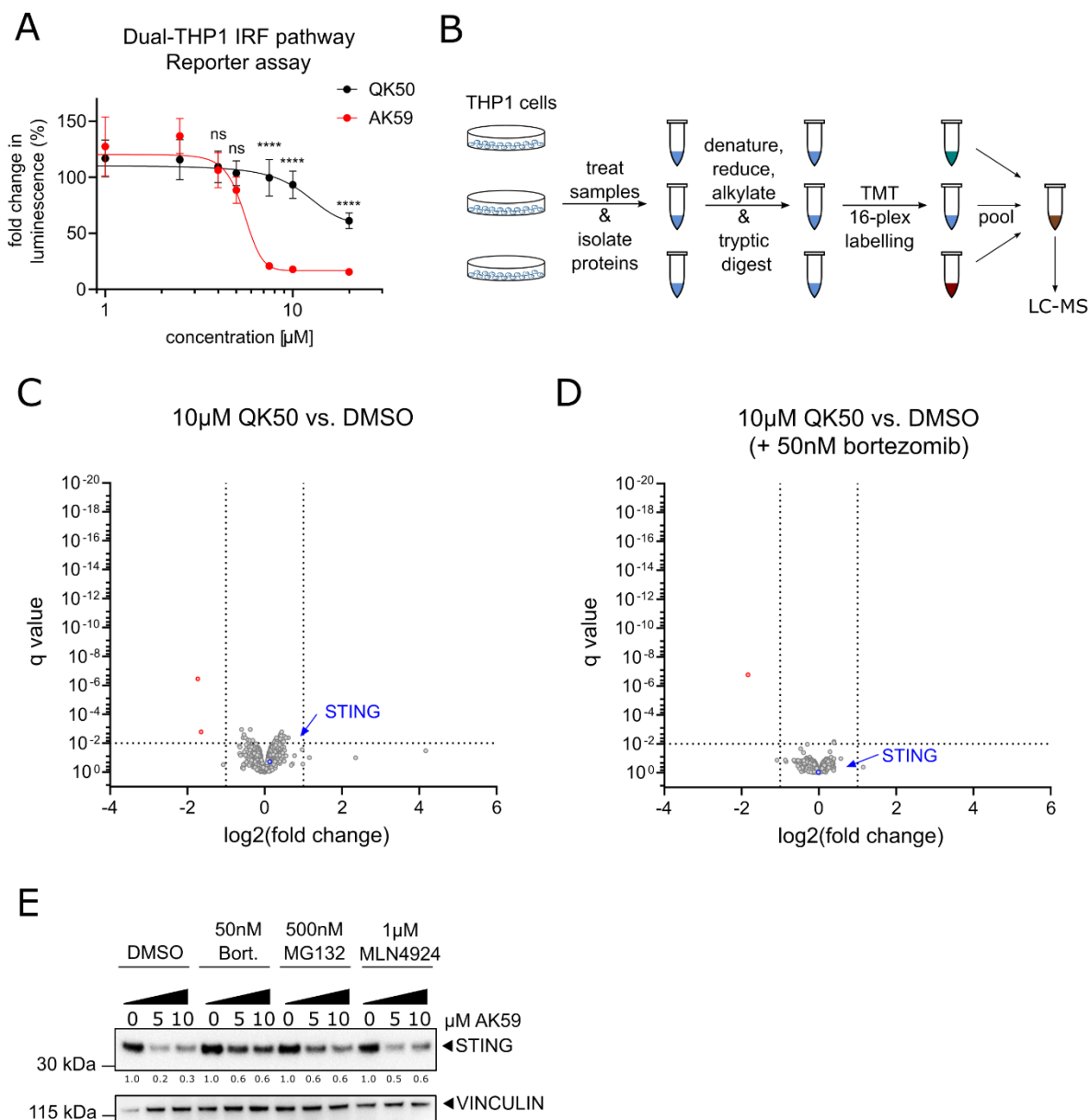
755 Supplementary Figure 5. Confirmation HERC4 knockouts in HEK293T and Dual-THP1 cells.

756 Supplementary Figure 6. Interaction of HERC4 and STING in the presence of AK59 treatment.

757 Supplementary Table S1. Proteomics results from either AK59 or QK50 treated THP1 cells.

758 Supplementary Table S2. CRISPR/Cas9 knockout screen RSA to Q values of hits.

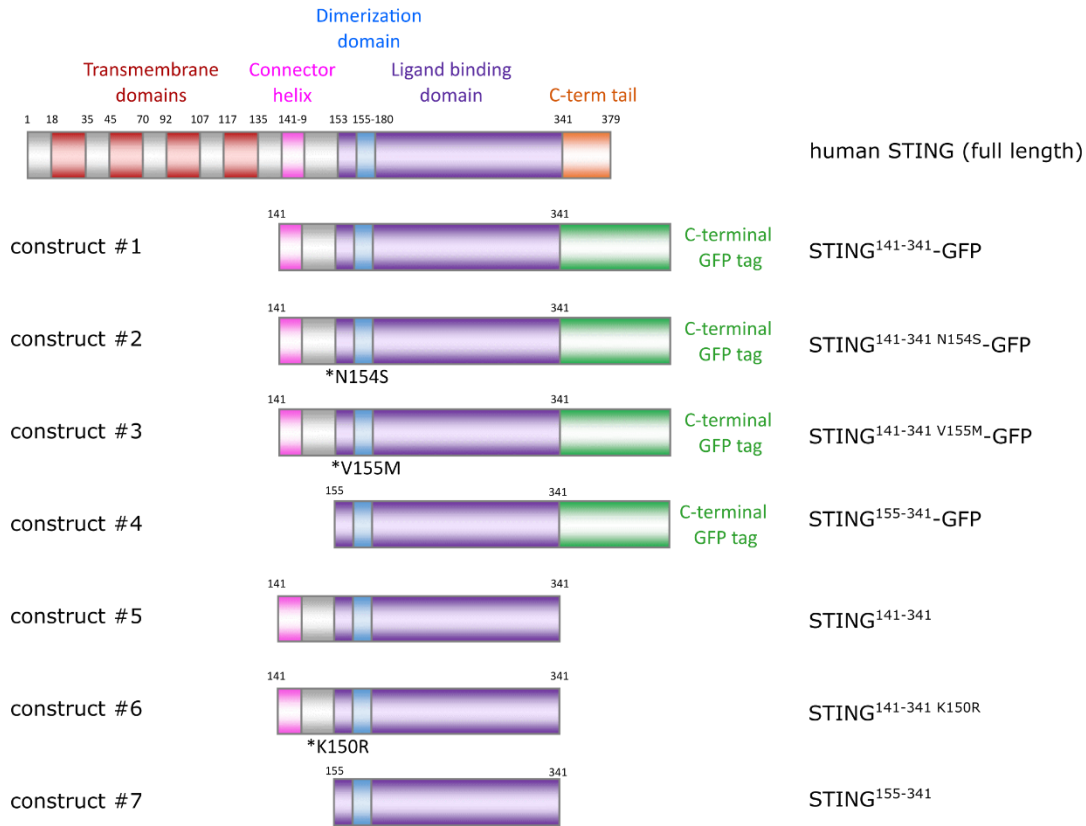




759

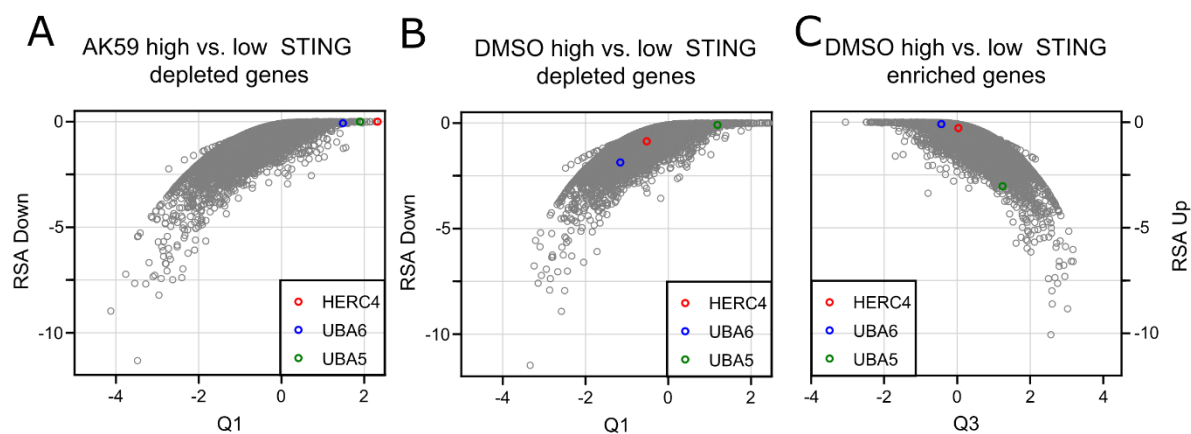
760 **Supplementary Figure 1. Compound characterization of AK59 and QK50.** (a) IRF pathway reporter assay on  
 761 wild type Dual-THP1 cells treated with either AK59 or QK50 for 16 hours. Cells were stimulated with 30 µM cGAMP  
 762 3 hours prior to compound incubation. Luminescence reads were normalized to the control unstimulated sample for  
 763 each cell line. Data plotted as mean ± SD of three individual biological replicates in Graphpad Prism (Version 9).  
 764 Statistical significance was calculated using two-way ANOVA followed by Šidák's correction. (b) Schematic  
 765 representation of proteomics on THP1 cells treated with either DMSO, AK59 or QK50. (c-d) Volcano plots of the  
 766 proteomics analysis of THP1 cells treated for 16 hours with 10 µM QK50 and with or without 50nM of bortezomib  
 767 treatment compared to matching DMSO control samples. Significantly altered protein abundances are shown with a  
 768 log<sub>2</sub> fold change < - 1 or > 1 and a q value of less than 0.01. (e) Western blot representing the changes in STING  
 769 expression upon AK59 and/or proteasomal inhibition (bortezomib or MG132) or neddylation inhibition (MLN4924)

770 in THP1 cells. VINCULIN used as a loading control. The STING expression quantified by first normalizing to its  
771 respective loading control and ratio to DMSO control.



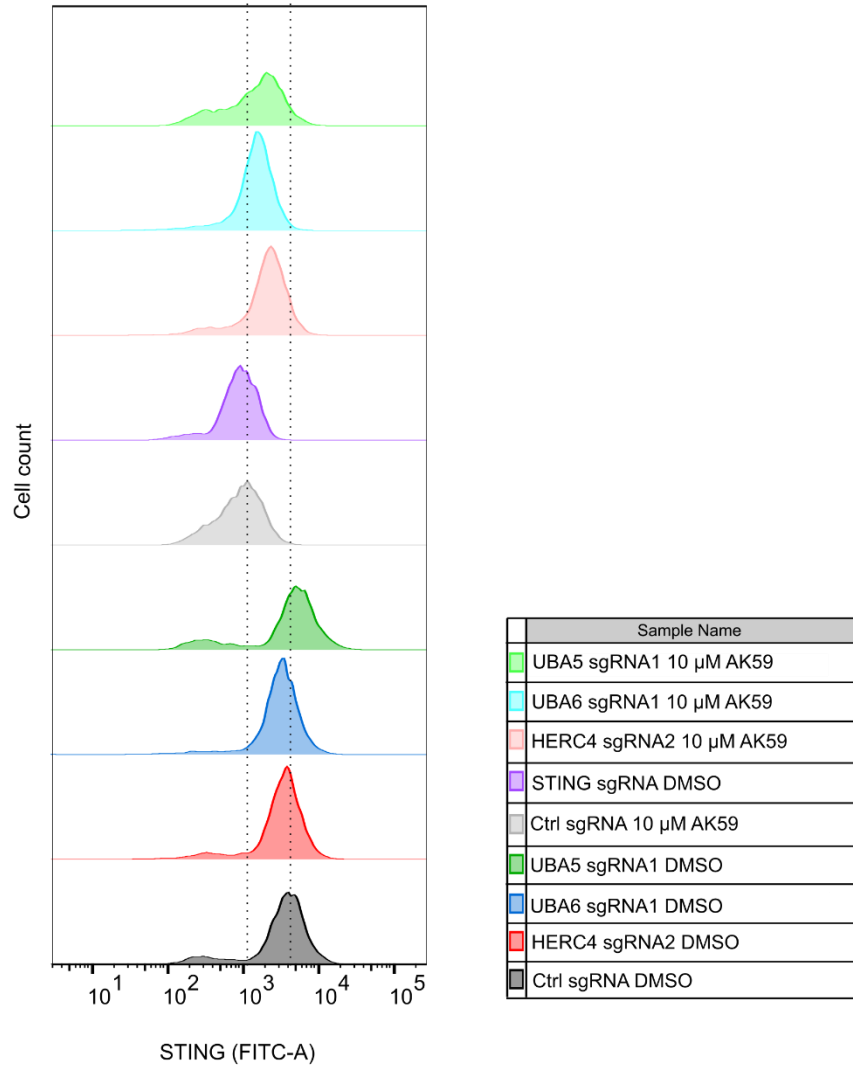
772

773 **Supplementary Figure 2. STING constructs.** Schematic representation of the STING constructs that are transiently  
774 expressed in HEK293T cells.



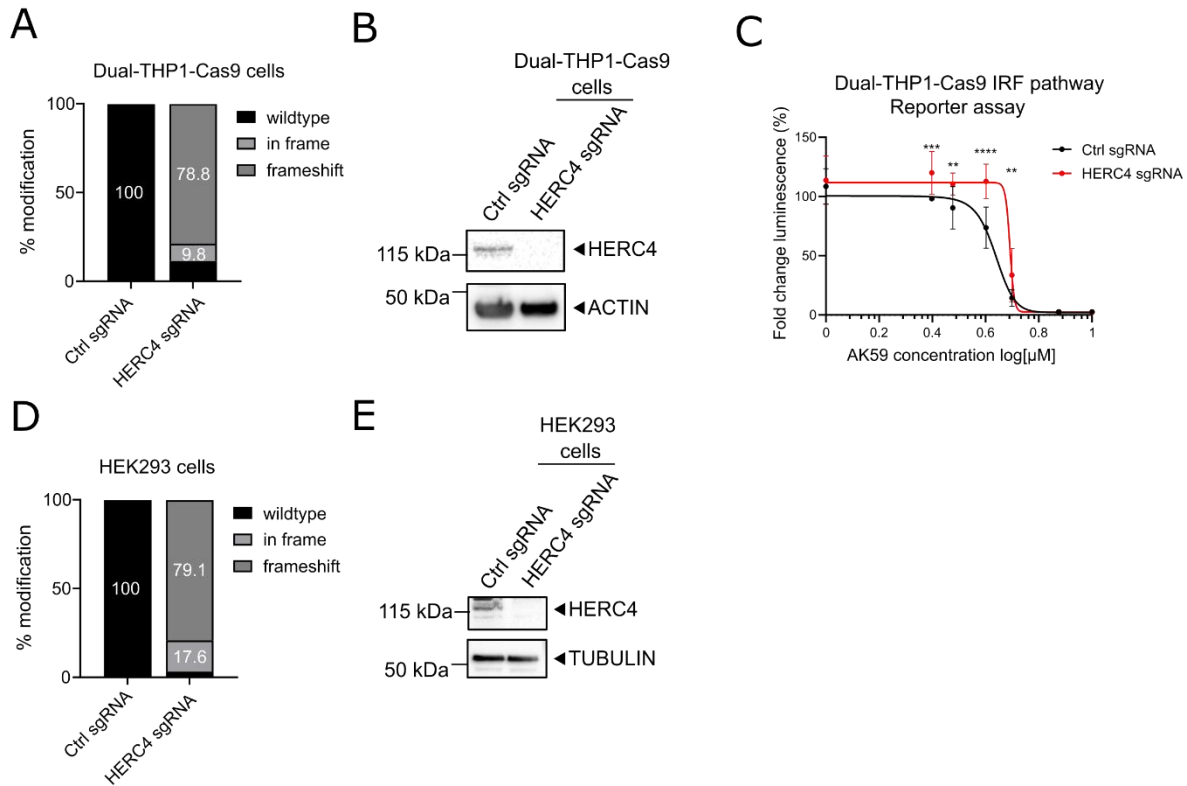
775

776 **Supplementary Figure 3. CRISPR/Cas9 genome-wide screening results.** (a) RSA down to Q1 values from  
777 CRISPR/Cas9 screen of 10  $\mu$ M AK59 treated THP1-Cas9 cells represented in a mustache plot. The comparison  
778 represented in the blot is high STING expression to low STING expression in the AK59 treatment group. Each dot  
779 represents a gene from the CRISPR/Cas9 library. (b) RSA up to Q3 values from CRISPR/Cas9 screen of DMSO  
780 treated THP1-Cas9 cells represented in a mustache plot. The comparison represented in the blot is high STING  
781 expression to low STING expression in the DMSO treated group. Each dot represents a gene from the CRISPR/Cas9  
782 library. (c) RSA down to Q1 values from CRISPR/Cas9 screen of DMSO treated THP1-Cas9 cells represented in a  
783 mustache plot. The comparison represented in the blot is high STING expression to low STING expression in the  
784 DMSO treated group. Each dot represents a gene from the CRISPR/Cas9 library.



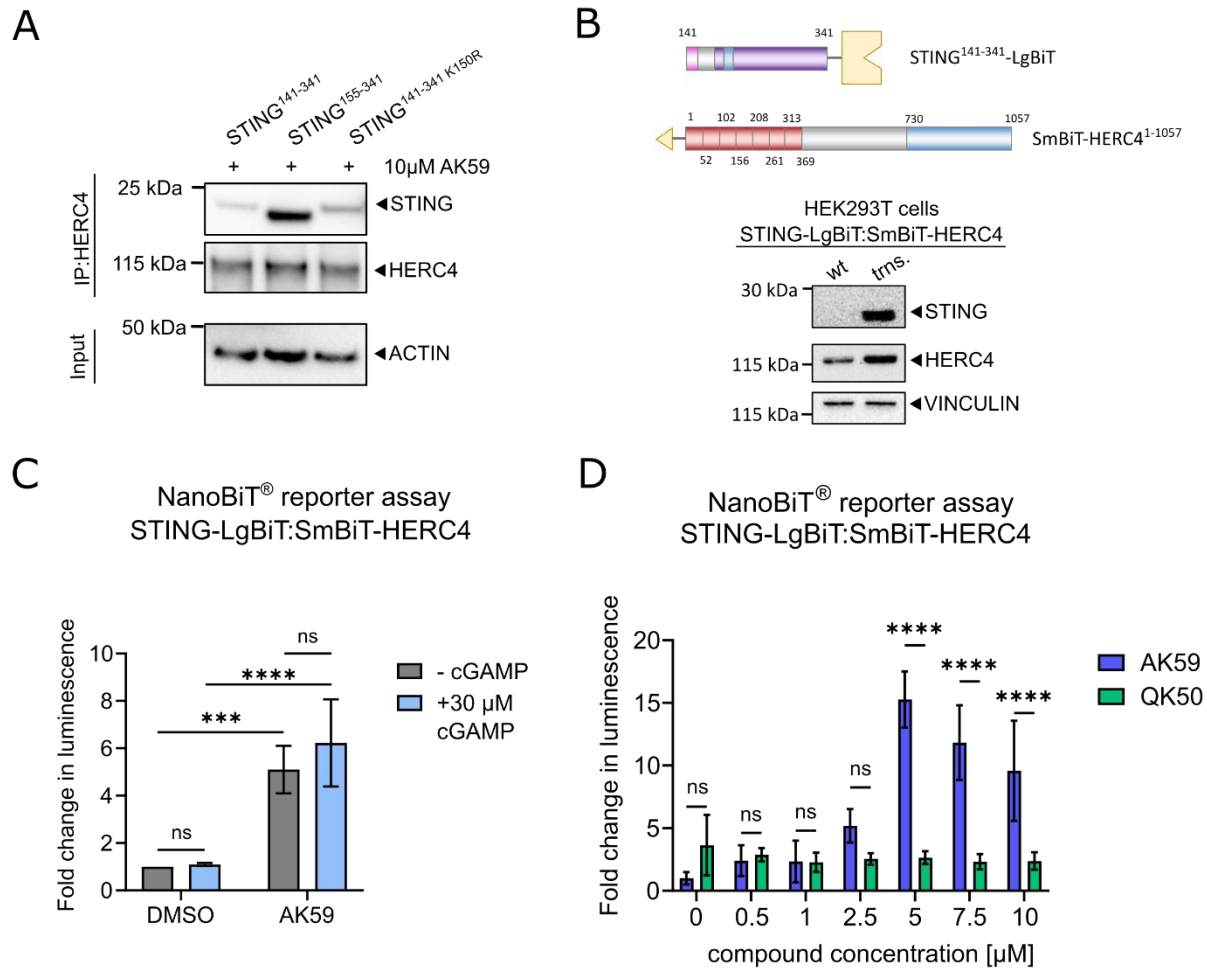
785

786 **Supplementary Figure 4. HERC4, UBA5 and UBA6 are validated as genes responsible in AK59 activity on**  
787 **STING expression.** FACS analysis of STING expression on Ctrl sgRNA, HERC4 sgRNA2, UBA6 sgRNA1 or  
788 UBA5 sgRNA1 transduces THP1-Cas9 cells that are treated either with DMSO or 10  $\mu$ M AK59. STING knockout  
789 line was taken along as a negative control (purple). Experiment treated at least in three biological replicates and  
790 representative FACS reads plotted using FlowJo (Version 10.6.1).



791

792 **Supplementary Figure 5. Confirmation HERC4 knockouts in HEK293T and Dual-THP1 cells.** (a) TIDE analysis  
 793 from either Ctrl sgRNA or HERC4 sgRNA1 transduced Dual-THP1-Cas9 cells. Modification rates were checked at  
 794 the third passage after the initial transduction. Undefined sequencing reads were excluded. (b) Western blot to detect  
 795 HERC4 protein levels on either Ctrl sgRNA or HERC4 sgRNA1 transduced Dual-THP1-Cas9 cells. Proteins from  
 796 each cell line collected at the third passage after the initial transduction. (c) IRF pathway reporter assay on wild type  
 797 or HERC4 knockout Dual-THP1-Cas9 cells. Cells were stimulated with 30  $\mu$ M cGAMP 3 hours prior to 16 hours  
 798 AK59 incubation. Luminescence reads were normalized to the control unstimulated sample for each cell line. Data  
 799 plotted as mean  $\pm$  SD of three individual biological replicates in Graphpad Prism (Version 9). Statistical significance  
 800 was calculated using two-way ANOVA followed by Šidák's correction. (d) TIDE analysis from either Ctrl sgRNA or  
 801 HERC4 sgRNA1 transduced HEK293-JumpIN-Cas9 cells. Modification rates were check at the third passage after  
 802 the initial transduction. Not defined sequencing reads were excluded. (e) Western blot to detect HERC4 protein levels  
 803 on either Ctrl sgRNA or HERC4 sgRNA1 transduced HEK293-JumpIN-Cas9 cells. Proteins from each cell line  
 804 collected at the third passage after the initial transduction.



805

806 **Supplementary Figure 6. Interaction of HERC4 and STING in the presence of AK59 treatment.** (a) HERC4  
 807 pulldown followed by western blot on HEK293T cells transfected with the indicated STING expression constructs  
 808 and treated with 10  $\mu$ M AK59. ACTIN was used as a loading and pulldown control. (b) Schematic representation of  
 809 the Nanobit constructs that were transiently expressed in HEK293T cells. Western blot showing the expression of  
 810 STING-LgBiT and SmBiT-HERC4 constructs in HEK293T cells. Comparison of wildtype (wt.) and transfected (trns.)  
 811 HEK293T cells. VINCULIN was used as a loading control. (c) Nanobit complementation assay on STING-LgBiT  
 812 and SmBiT-HERC4 expressing HEK293T cells in the presence of AK59 and/or cGAMP. 30  $\mu$ M of cGAMP  
 813 stimulation was done 3 hours prior to indicated compound treatments. DMSO were used as a negative control and  
 814 luminescence reads were normalized to corresponding DMSO control. Three biological replicates were plotted as  
 815 mean  $\pm$  SD using in Graphpad Prism (Version 9). Statistical significance was calculated using two-way ANOVA  
 816 followed by Šidák's correction. (d) Nanobit complementation assay on STING-LgBiT and SmBiT-HERC4 expressing  
 817 HEK293T cells in the presence of increasing concentration of either AK59 or QK50. Biological replicates were plotted  
 818 as mean  $\pm$  SD using in Graphpad Prism (Version 9). Statistical significance was calculated using two-way ANOVA  
 819 followed by Šidák's correction.